Mechanical Design of a Trawl-Resistant Self-Mooring Autonomous Underwater Vehicle

Taylor B. Wilson

Thesis submitted to the Faculty of the
Virginia Polytechnic Institute and State University
in partial fulfillment of the requirements for the degree of

Master of Science
In
Ocean Engineering

Wayne L. Neu, Chair
Daniel J. Stilwell
Craig A. Woolsey

December 8, 2015
Blacksburg, VA

Keywords: Autonomous Underwater Vehicle, Self-Mooring, Trawl-Resistant, AUV, TRSMAUV

Mechanical Design of a Trawl-Resistant Self-Mooring Autonomous Underwater Vehicle

Taylor B. Wilson

ABSTRACT

The Virginia Tech Trawl-Resistant Self-Mooring Autonomous Underwater Vehicle (TRSMAUV) is designed to reside on the seafloor for extended periods of time. The TRSMAUV shape allows for deployment in areas where trawl fisheries are conducted. TRSMAUV is a two stage vehicle. The ingress vehicle is the delivery device, and it is constructed from two symmetric halves. The top half contains the ingress vehicle propulsion system and control surfaces. The bottom half is the trawl-resistant mooring package. A smaller vehicle, the egress vehicle, is housed within the bottom ingress half and provides the guidance, navigation and control algorithms for the TRSMAUV. This report covers the general design elements of the TRSMAUV, the detail design of several prototypes, the results of the field trials, and the next steps that will be taken to build the final vehicle.

Acknowledgments

I would first like to thank the rest of the design team of the TRSMAUV project. This was a very long and complicated project, and many graduate students made sizable contributions. Every team member contributed ideas to parts of the process that may or may not have been within their technical field. I also cannot thank Dr. Neu and Dr. Stilwell enough, they contributed advice and ideas throughout every stage of the vehicles development. I would also like to extend a thank you to the engineering team at the Naval Oceanographic Office. They provided a significant amount of technical support and this project would not have been possible without them.

Contents

List of Figures

List of Tables

List of Abbreviations

AHRS:	attitude, heading and reference system
AUV:	autonomous underwater vehicle
CAD:	computer assisted drawing
CB:	center of buoyancy
CEP:	circular error probable
CFD:	computational fluid dynamics
CG:	center of gravity
COTS:	commercial off the shelf
CPU:	central processing unit
FEA:	finite element analysis
GPS:	global positioning system
LED:	light emitting diode
MATLAB:	matrix laboratory (software)
RPM:	rotations per minute
VT-SMAUV:	Virginia Tech Self-Mooring autonomous underwater vehicle
TRSMAUV:	Trawl-Resistant Self-Mooring autonomous underwater vehicle

1 Introduction

The Autonomous Systems and Controls Laboratory at Virginia Tech developed an Autonomous Underwater Vehicle (AUV) that is capable of traveling to a location and anchoring itself on the sea floor to collect data (the Virginia Tech Self-Mooring AUV). It is desirable to have such an AUV capable of mooring itself in locations where commercial trawl fisheries occur. To achieve this, the AUV must be both self-mooring and trawl-resistant. For an AUV to be trawl resistant when moored, it must mimic the characteristics of other trawl-resistant bottom-mounted devices. These devices are able to deflect trawls (e.g., trawl footropes, roller gear, bridles) without sustaining damage. The Virginia Tech Trawl-Resistant Self-Mooring Autonomous Underwater Vehicle (TRSMAUV) is designed for this purpose.

The TRSMAUV is a two stage vehicle. The ingress vehicle is the delivery device, and it is constructed from two symmetric halves. The top half contains the ingress vehicle propulsion system and control surfaces. The bottom half is the trawl-resistant mooring package. A smaller egress vehicle is housed within the bottom ingress half and provides the guidance, navigation and control functions for the TRSMAUV.

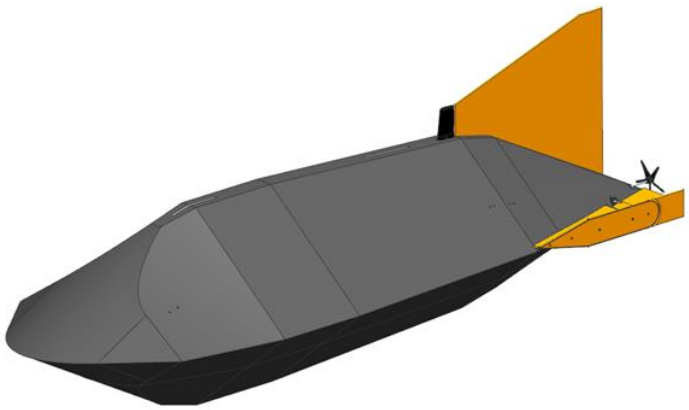

Figure 1.1: TRSMAUV in the initial deployment state

The TRSMAUV will navigate to a predetermined mooring location and execute a controlled descent to the sea floor. Before the vehicle reaches the bottom, the two halves will separate and the bottom half will settle to the sea floor in an inverted state to achieve a low-relief, trawl-resistant profile. The vehicle is designed to deflect trawl cables at speeds $\leq$ 4 knots. Design criteria also specify that the TRSMAUV can remain moored for up to one year at depths $\leq$ 500 m. Upon completion of the moored period, the egress vehicle is released from the TRSMAUV bottom half and returns to a recovery location.

The egress vehicle design was based on the existing Virginia Tech Self-Mooring AUV (VT-SMAUV). This paper details the design of the ingress vehicle, the construction of a prototype ingress vehicle, the construction of the egress vehicle, and field testing of both vehicles.

1.1 Mission Profile

The TRSMAUV mission profile can be separated into eight different phases: 1) Ingress, 2) Buoyancy Release, 3) Helical Descent, 4) Separation, 5) Landing, 6) Top Half Release, 7) Egress Vehicle Release, and 8) Egress.

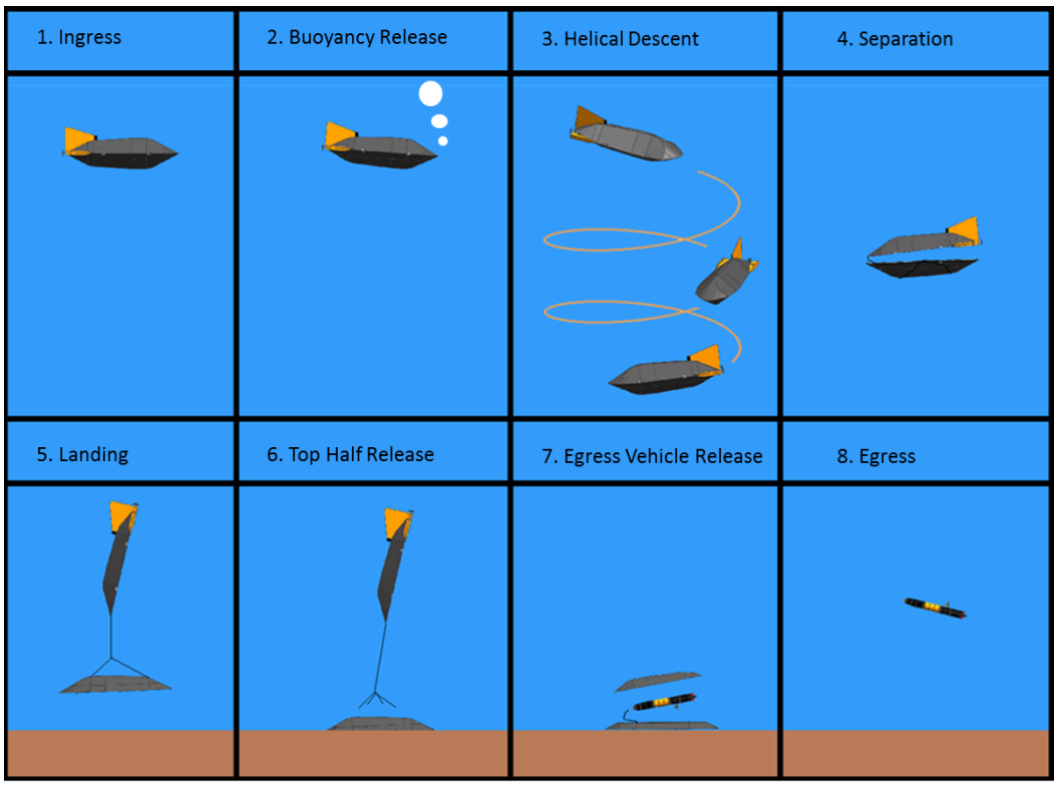

Figure 1.2: The eight different phases of the TRSMAUV mission profile

During the ingress phase the TRSMAUV is deployed and swims to a predetermined location. The TRSMAUV has a range of $\leq$ 50 nautical miles and can be deployed in areas where a head current of $\leq$ 0.5 m/s is present. The vehicle is designed to cruise at a speed of 2 m/s at a depth of 3 m. When the vehicle arrives at the designated surface location, buoyancy is released to alter the vehicle's buoyancy state. This release gives the vehicle a negative net buoyancy (roughly 10%) for the descent phase. The vehicle then begins a controlled helical descent to a depth $\leq$

500 m. As the vehicle nears the sea floor the two halves separate at a user-defined depth. The two halves remain in a temporary state of attachment so that the bottom half is allowed to roll over and descend in an inverted state. This allows the buoyant top half to act as a drogue for the heavy bottom half. The bottom half will gently come to rest on the seafloor in this inverted state to achieve the trawl-resistant profile. Once the bottom half settles to the sea floor, the disposable top half is released and drifts away.

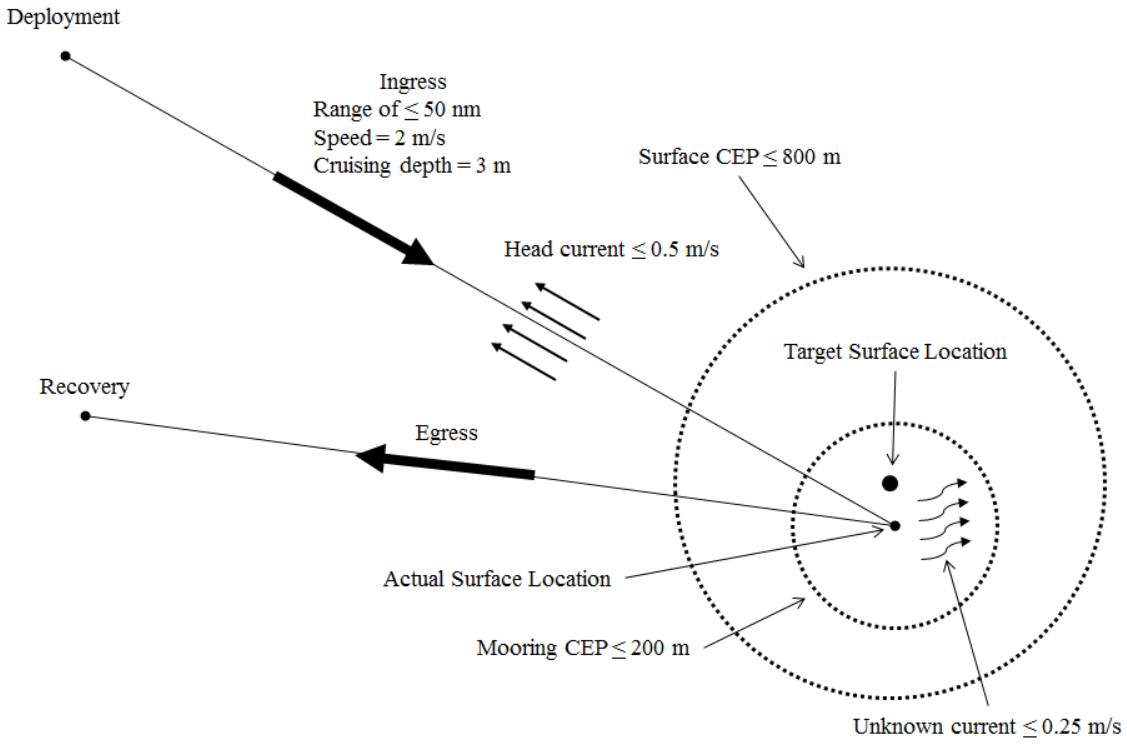

Figure 1.3: Schematic of mooring mission profile (not to scale)

Design parameters specify the TRSMAUV must land within a 200 m circular error probable (CEP) of its last GPS fix even when subject to an unknown current with a magnitude $\leq$ 0.25 m/s. The final moored position will be within 800 m of the desired location (Fig. 1.3). The vehicle can remain in its moored state for up to one year. The egress vehicle is released upon completion of the data collection period, and autonomously navigates to the desired recovery location for extraction.

1.2 Design Approach and Team Structure

The TRSMAUV is designed as a trawl-resistant mooring device for integration with the existing Virginia Tech Self-Mooring AUV (VT-SMAUV) [5]. This integrated package required slight modifications to the VT-SMAUV for use as an egress vehicle and the design of a new trawl-resistant ingress vehicle. Designing the overall shape of the ingress vehicle was the first challenge. This overall profile had to meet specific design requirements. That is, the ingress vehicle needed to house the egress vehicle (modified VT-SMAUV), while maintaining a specified profile and weight to be trawl-resistant. Once the exterior shape was chosen, ingress vehicle subsystems were developed. When final concepts were attained, a scale prototype of the ingress vehicle was built to test the separation and landing phases. After these concepts had proven successful, a full size, limited capability prototype was built to test the full scale separation, landing, and trawl-resistant performance. Ingress vehicle detail design work was completed following successful field tests. A prototype ingress vehicle was then built to test the flight ability and full ingress vehicle mission.

The final egress vehicle (Fig. 1.4) was built in parallel to the ingress vehicle redesign and development work. Furthermore, both ingress and egress field tests were conducted alongside one another. The next phase of the project will involve integration of the ingress and egress vehicles, and full mission field tests.

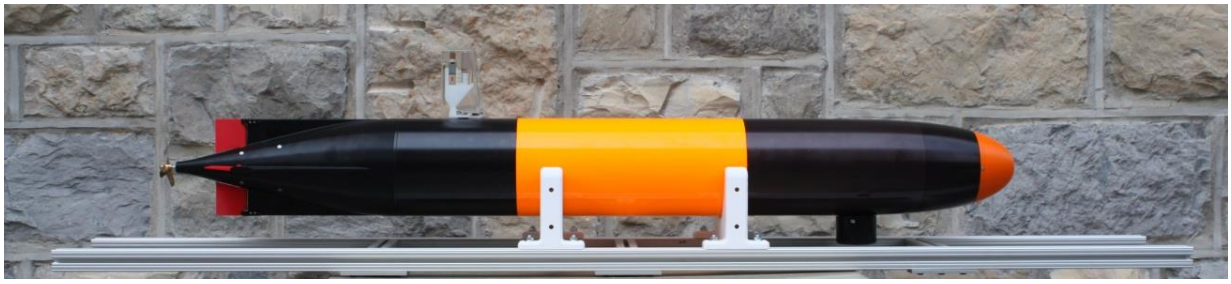

Figure 1.4 Egress vehicle

The design team for the TRSMAUV consists of Virginia Tech students and faculty in both the Department of Aerospace and Ocean Engineering, and the Bradley Department of Electrical Engineering. The design process for the TRSMAUV was lengthy, and many students contributed to different phases of the development. Faculty members Dr. Dan Stilwell and Dr. Wayne Neu were responsible for project conception and contributed to all phases of the design process. Brian McCarter, Stephen Portner, Rand Pearson and Eddie Ball completed the general conceptual design of the TRSMAUV system (Sections 2.2.1, 2.2.3). Following general concept design, TRSMAUV development was broken down into two components: design of the egress vehicle and design of the ingress vehicle. S. Portner completed both conceptual and detail design of mechanical and propulsion systems of the egress vehicle (Sections 2.2.4, 5.1 and 5.2). The electrical design was primarily B. McCarter, with assistance from Scott Gibson and Maria

Khater. S. Portner completed conceptual mechanical design of the ingress vehicle (Sections 2.2.3.3 and 2.2.4). Additionally, S. Portner completed detail design work for both the ingress scale model and ingress limited prototype (Chapters 3 and 4). Taylor Wilson performed the detail mechanical design of the final ingress vehicle prototype (Chapter 6), with assistance from E. Ball. This included design of mechanical components for various subsystems and integration of subsystems into the prototype vehicle. T. Wilson performed structural analysis using finite element analysis (FEA) methods where applicable (Sections 6.5 and 6.6). B. McCarter performed initial electrical design, while S. Gibson completed detail electrical design, with assistance from M. Khater. Ingress vehicle propulsion system design was handled primarily by E. Ball (Section 6.2). Computational fluid dynamic (CFD) analysis of both the ingress and egress vehicles was completed by E. Ball (Sections 2.2.2, 6.1 and 6.3)

1.3 Thesis Layout

This thesis covers the various phases of the TRSMAUV design process, with the focal point being the mechanical design of the ingress vehicle prototype. The first few chapters cover elements of the process that lead up to the mechanical design of the ingress vehicle prototype. This background information includes: chapter 2, which covers general conceptual design of the TRSMAUV, as well as conceptual design of some of the subsystems; chapter 3, which covers the building and testing of a scale model ingress vehicle; chapter 4, which covers the design, building and testing of a full size limited ingress vehicle prototype; and chapter 5, which covers the design, building and testing of the egress vehicle. Chapter 6 is the focus of this paper and covers the detail mechanical design work for the ingress vehicle prototype. Chapter 7 covers the next stages that are required to complete the TRSMAUV project.

2 Conceptual Design

The initial concept was to design a trawl-resistant mooring capability for the existing Virginia Tech Self-Mooring AUV. A detailed description of the original VT-SMAUV can be found in [5]. The trawl-resistant concept required the development of an ingress vehicle that could be moored on the seafloor. The ingress vehicle would house an egress vehicle of similar design to the VT-SMAUV. The ingress vehicle would rely on the egress vehicle for many functions. The ingress vehicle will display the principle characteristics of a traditional trawl-resistant mount (Fig. 2.1) in addition to having an exterior shape consistent with controlled flight. The ingress vehicle needs to perform several functions during the mission profile described in section 1.1. Conceptual ideas for these capabilities are described in the following sections of this document. Several modifications were made to the VT-SMAUV design to produce the egress vehicle. The conceptual ideas behind these modifications are also briefly described in this document.

Figure 2.1 Traditional trawl-resistant mooring manufactured by Mooring Systems, Inc [9]

2.1 Egress Vehicle

As few modifications as possible were made to the VT-SMAUV to minimize the engineering effort required to design and build a suitable egress vehicle. The two largest modifications were to the power budget and the nose design of the vehicle. The egress vehicle only needs to carry

enough power to complete the egress portion of the mission as described in Section 1.1. This is because the egress vehicle will draw from the ingress vehicle batteries during the ingress mission phase. This power sharing feature enabled the Team to reduce the overall length of the VT-SMAUV from 74 to 61 inches. The important modification to the nose design occurred as the egress vehicle no longer needs to carry the false nose as a mooring anchor. Instead, the nose must contain an electrical connection to the ingress vehicle. This "umbilical" is disconnected to complete the egress vehicle release phase of the mission.

Figure 2.2 Virginia Tech Self-Mooring AUV shown without the false nose, which functions as a mooring anchor

2.2 Ingress Vehicle

The TRSMAUV ingress vehicle has far more design constraints than a typical general purpose AUV. This is necessary as the vehicle must be both trawl-resistant and capable of efficient, controlled flight. It is possible to generally consider the internal components necessary for the ingress vehicle into the following categories:

1. The egress vehicle: The egress vehicle size is reduced by making the modifications described in Section 2.1 to the VT-SMAUV. This vehicle will still host the payload, most electronics, and all computational hardware/software. All guidance and control functions will reside in the egress vehicle.

2. Disposable buoyancy: The ingress vehicle is only required to be positively buoyant during the ingress portion of the mission. Inexpensive pressure bottles can be used to store air as buoyancy as this will occur at shallow depths.

3. Batteries: The ingress vehicle will house all batteries necessary for all phases of the mission profile except the egress phase.

4. Propulsion and control systems: The ingress vehicle will need its own propulsion system and control surfaces to navigate to the mooring location and successfully descend to the sea floor. These systems can be inexpensive because they will be primarily operated near the sea surface.

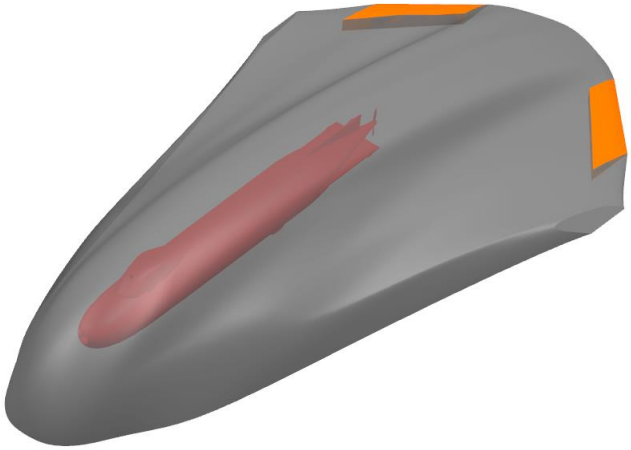

Figure 2.3 Hypothetical ingress vehicle [7]

2.2.1 Exterior Shape Design

The design of the exterior shape of the ingress vehicle must incorporate the trawl-resistant bottom mount requirements. This design was based on conventional trawl-resistant systems. Review of earlier work to develop trawl-resistant bottom mounts showed several common features to consider. The overall size of the bottom mount also had to be sufficient to house the egress vehicle.

1. Wet weight while moored: Wet weight can be specified as the force exerted over the bottom surface area of the trawl-resistant mount while moored. Bottom force per surface area in previous reported trawl-resistant mount designs ranges from 0.03-0.08 psi [1-3].

2. Side slope: The sides of trawl-resistant bottom mounts have a shallow slope so that trawl cables are passively directed over the mount. The slope relative to the horizontal ranges between 25 and 40 degrees ([1] and [2] respectively) in previous trawl-resistant mount designs.

3. Bottom structures: The underside of the bottom mount is occasionally equipped with a vertical lip. In the case of the Barney trawl-resistant bottom mount, a downward projecting lip around the circumference of the mount is used in muddy conditions, but is omitted for sandy bottoms [3]. In the case of the MSI trawl-resistant bottom mount, the frustum-shaped cover rests upon a 1 inch thick gridded panel base, which may reduce settling into soft sediments of the seafloor [2].

The wet weight while moored and the side-slope are principle design constraints. As the ingress vehicle must originally be neutrally buoyant, the buoyant force of the disposable buoyancy is dependent on the desired wet weight while moored. The desired wet weight will be chosen based on the appropriate bottom pressure.

In addition to bottom wet weight and side slope, consideration was given to the following criteria:

1. Minimum dry weight and size to make handling and deployment as easy as possible
2. Physical robustness sufficient to survive impact by trawl itself (e.g., trawl footrope, mud gear, roller gear) or trawl components (i.e., trawl bridle, trawl door)
3. Minimum cost for unrecoverable components
4. Use of nonmagnetic materials

2.2.2 Preliminary Hydrodynamic Analysis

A preliminary hydrodynamic analysis of the ingress vehicle was performed to determine if the device could achieve controlled flight. The exterior shape of the vehicle is dramatically different from other submersible vehicles. Computational fluid dynamic (CFD) methods were used to conduct the analysis [6].

2.2.2.1 Shell Design

It was necessary to have an accurate CAD model of the ingress vehicle exterior shape for the CFD analysis. A notional shell was designed based on the trawl-resistant design constraints described in Section 2.2.1, the estimated size of the egress vehicle, and basic hydrodynamic principles. This shell profile would be used in all of the CFD analysis to determine hydrodynamic feasibility.

The notional shell is depicted in Fig. 2.4. The maximum sideslope of the shell is 37.5 degrees, while the minimum sideslope is 27.1 degrees. This kept the sideslope well within the trawl-resistant parameters (described in Section 2.2.1) while maintaining a hydrodynamic design. An initial wet weight was chosen so that the bottom pressure would be 0.03 psi. This value is at the minimum of the valid bottom pressures. It was chosen to reduce the overall weight of TRSMAUV. Reduction of the overall weight reduces the amount of buoyancy to add to the ingress vehicle and reduces out-of-water handling difficulties.

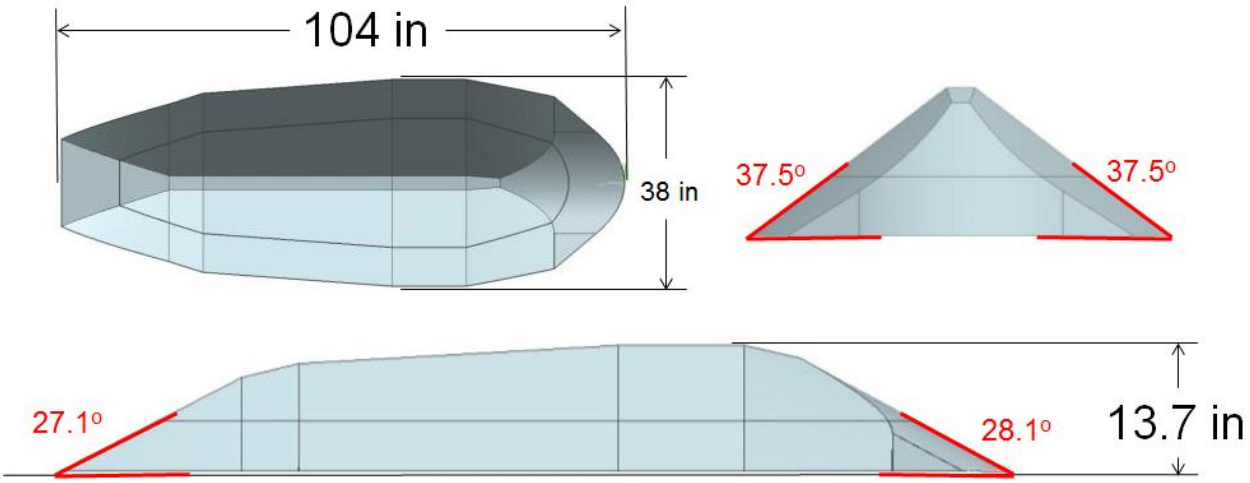

Figure 2.4 Exterior shell dimensions for the ingress vehicle

2.2.2.2 CFD Analysis

The CFD simulation determined the hydrodynamic effects on the body when fully submerged and traveling at 2 m/s through water. It was evident that using such a drastically asymmetric body generated a large pitching moment, which would be very difficult to control. This pitching moment is a result of the lift and drag forces experienced by the body, and is illustrated in Fig. 2.5.

The initial ingress vehicle generated:

1. Drag = 67.37 N @ 2 m/s
2. Lift = 259.1 N @ 2 m/s
3. Pitch Moment = -255.6 N-m (about approx. centroid of vol.) @ 2 m/s

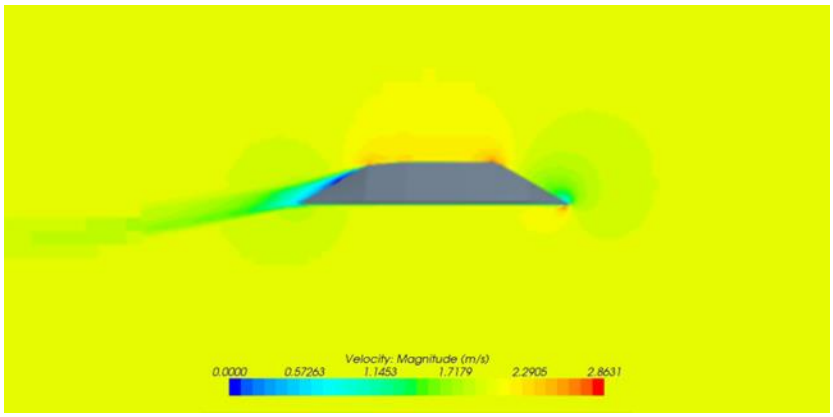

Figure 2.5 CFD results from the one-sided ingress vehicle [6]

The proposed solution to minimize pitching was to mirror the shell, creating a double sided body with horizontal plane symmetry. This created a more stable body that would reduce control and propulsion difficulties. The CFD analysis indicated that this body experienced significantly less drag, which resulted in a more efficient vehicle (Fig. 2.6).

The two sided version of the ingress vehicle generated:

1. Drag = 54.6 N @ 2 m/s
2. Lift = 0 N @ 2 m/s
3. Pitch Moment = 0 N (about approx. centroid of vol.) @ 2 m/s

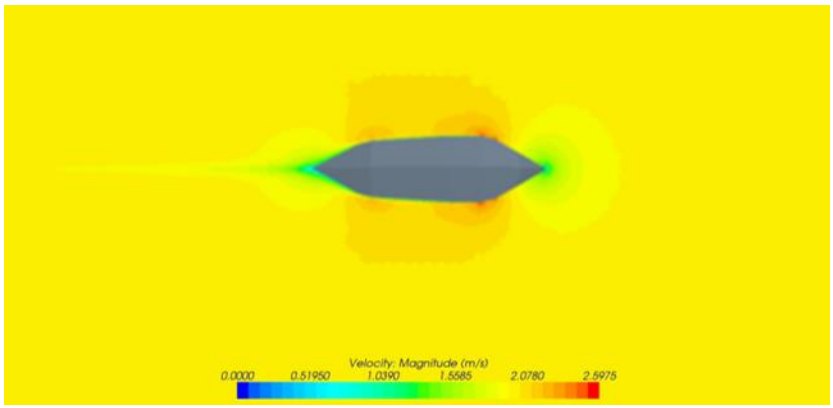

Figure 2.6 CFD results for double sided symmetric body [6]

The hydrodynamic analysis clearly demonstrated that a body with horizontal plane symmetry was desirable. This increased the overall complexity for the ingress vehicle and TRSMAUV because only half of the body was required for mooring.

2.2.3 Overall Systems Layout

Using two symmetric halves for the ingress vehicle introduced more design complications. The bottom half would be the mooring package. It would be heavier than the water it displaced and would be positioned on the bottom of the ingress vehicle to ensure roll and pitch stability. Most of the bottom half design would be constrained by the requirements generated in Section 2.2.1. It was important to place control surfaces, propellers, and any other external structures needed for flight and communication in the top half to minimize the vertical relief of the bottom half and thus maximize the trawl-resistance. The weight of the full ingress vehicle is conditional on the desired wet weight of the bottom-half mooring package. To maintain stability and obtain the desired buoyancy for the complete ingress vehicle, all of the positive buoyancy must be located in the top half. The ingress vehicle must mechanically separate the halves and perform passive descent and landing on the sea floor.

2.2.3.1 Buoyancy Control

As described in Section 2.2, a large portion of the buoyancy in the ingress vehicle will be disposable. This buoyancy is only required at shallow depths so air tanks will not be subject to the large crush pressures that exist at greater depths. These air tanks will be flooded prior to the helical descent stage of the mission. The tanks will be located within the ingress vehicle and thus will be part of the disposable portion of the TRSMAUV. When designing these buoyancy tubes several design constraints were considered:

1. Minimum cost: These components will be part of the disposable ingress vehicle and will be made from readily available materials that are cost effective and easy to machine (i.e. PVC pipe).

2. Simplicity and reliability: Failure to flood could compromise the entire mission

3. Rapid flooding: To deploy the TRSMAUV where large currents may be present, it is necessary to execute the buoyancy release and helical descent as rapidly as possible. This will increase the chance that the vehicle lands within the CEP.

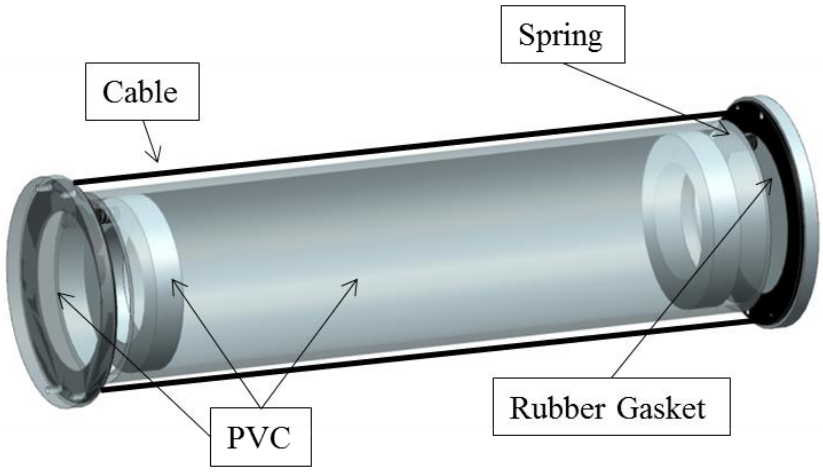

Figure 2.7 Hypothetical air tube utilizing an internal spring to open bulkheads and initiate flooding.

Figure 2.7 shows a conceptual buoyancy release tube. This tube has two bulkheads that use face seals to mate with a hollow tube. A cable can be used to hold the bulkheads in place. Two small springs will be held in compression when the bulkheads are mated with the tube. By cutting the cable the springs will overcome hydrostatic pressure and release both end caps, causing the tube to flood.

2.2.3.2 Propulsion and Control

Conceptual design of the propulsion system began following the ingress vehicle CFD results. Overall drag was used to determine thrust for the desired cruising speed. CFD analysis was then used to determine the velocity inflow profile for different propeller positions based on the flow over the bare ingress vehicle shell. OpenProp and Matlab were used to optimize the propulsion design using several variables [6]. The variables included:

1. Motor – More than 25 commercial of the shelf (COTS) motors were evaluated.
2. Propeller Diameter – Varied in one inch increments to a maximum of 60% of the ingress vehicle height.
3. RPM – Varied in increments of 100 between 800 and 10000 and increments of 1000 between 11000 and 50000.
4. Gear ratio – Standard gear ratios based on available gear boxes for each COTS motor were considered.
5. Peak battery voltage – Varied based on different combinations of individual cells of different battery compositions (i.e. lithium polymer vs. alkaline).
6. Number of Blades – Three and five bladed propellers were considered.

The general procedure is outlined below:

1. Use CFD to determine velocity inflow profile and vehicle drag profile
2. Use OpenProp to determine torque vs rpm curves for each propeller diameter and number of blades
3. Use a Matlab script to match each COTS motor with each propeller diameter by finding the intersection of torque vs. rpm propeller curve with torque vs. rpm motor curves. This is completed over a combination of assumed battery voltages and gear ratios.
4. Calculate overall efficiency of each motor/propeller combination

The initial analysis compared the optimal efficiencies of a single propeller versus two propellers without regard to the wake of the body. A slight increase in efficiency was shown in the single propeller design. This gain was considered small enough to be within the uncertainty bounds of the optimization design results. The twin screw arrangement was chosen for this reason, and the fact that twin screw design would enable the TRSMAUV to control yaw using differential thrust.

Table 2.1 OpenProp optimization results [6]

	Single Propeller	**Two Propeller**
Motor	Neumotor – 1924/3Y/6MM	Neumotor – 1924/3Y/6MM
Diameter (in)	12	10
Gear Ratio	1	1
Peak Voltage (v)	11.55	9.9
Number of Blades	3	5
Propeller RPM	1350	1200
Torque on Prop (oz-in)	84.895	52.430
Total Efficiency	0.84	0.77

Two twin screw configurations were evaluated: An inboard design, positioning the propellers at opposite ends of the trailing edge of the vehicle, and an outboard design, with symmetric motor pods mounted on the aft section of the vehicle (Fig. 2.8).

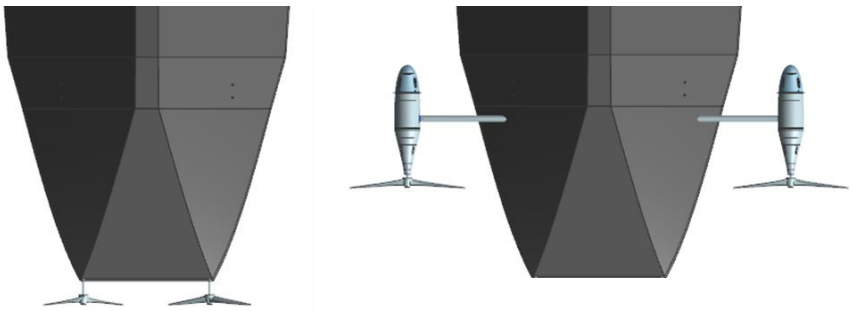

Figure 2.8 Conceptual inboard (left) and outboard (right) propulsion system configurations.

The outboard configuration offered several benefits over the inboard design: 1) External motor pods could rotate for pitch control, removing the need for elevators. 2) Increased propeller spacing would lead to a finer turn radius. However, these external pods would have a negative effect on the overall drag of the vehicle and could reduce overall propulsive efficiency. The mechanical integration of the outboard pods was considered to be more complicated than the inboard configuration.

The inboard design reduces drag, however each propeller will be operating in the wake of the vehicle thus reducing propeller efficiency. This design requires the addition of external flaps for pitch control. Final propulsion design (Section 6.2) was completed following validation of some of the novel mechanical/hydrodynamic systems in the ingress vehicle. Many design features had to be completed and validated prior to detail propulsion design.

2.2.3.3 Attachment & Separation

Another system introduced into the two body ingress design is the attachment/separation mechanism of the two halves. The two halves of the vehicle must be fastened together with enough strength to resist several forces. This connection will experience a large static load generated by the difference in buoyancy of the top and bottom halves (estimated as 250 lbs). There will also be hydrodynamic forces induced on the body while it is underway. In addition to these known loads, additional dynamic loads could be exerted on the vehicle during initial deployment and must be considered.

The connections between the two body halves must be reliably severed to allow successful completion of the separation phase of the mission. Failure of this phase would result in mission failure and potential loss of the egress vehicle.

Some of the principal mechanisms evaluated for use as the separation connection are listed below:

1. Latch Mechanism: Several latches were considered necessary to connect different points of the top and bottom halves. Each latch would be released by a servo either independently or simultaneously.
2. Pyrotechnic Mechanism: Use of exploding bolts, similar to those used in rocket stage separation, were considered.
3. Non-Pyrotechnic Release Actuator: Use of one or several actuators specifically designed to release fasteners were considered.

The latch mechanism was selected for preliminary testing. This was chosen primarily because it proved to be extremely cost effective. That is, it was the least expensive mechanism that was

robust, simple and highly reliable. Pyrotechnic mechanisms can be cost effective, however they are often considered “live ammunition” and can add complication to handling and deployment regulation.

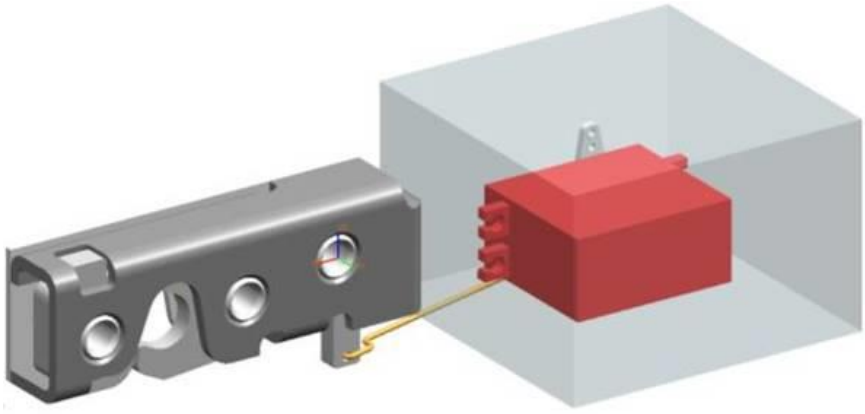

Figure 2.9 Hypothetical separation mechanism [7]

The hypothetical latch mechanisms consisted of a rotary latch linked to a servo enclosed in a watertight housing (Fig. 2.9). The rotary latch secures to a pin in the opposing half. By actuating the servo the linkage transmits the force to the latch release lever and releases the connection.

2.2.3.4 Mooring

The ingress vehicle can no longer be actively controlled after separation of the halves. Several different decent and mooring methods were considered. Considered landing requirements included:

1. Land within a 200 m CEP of the last GPS fix assuming an unknown current with a magnitude of ≤ 0.25 m/s
2. Soft landing to prevent damage to hull or components.
3. Mooring package correctly oriented to achieve trawl-resistant state.

Several options were investigated based on these criteria. Time of separation is critical because the ingress vehicle will lose control authority after separation. Simulation studies determined that an uncontrolled descent from the surface would not be reliable enough to result in a soft landing within the required CEP. Separation must occur near the sea floor. This would allow the ingress vehicle to be controlled for the majority of the descent.

After separation of the two halves, the bottom mooring package must invert and descend to the sea floor. Three options were considered to carry out this phase of the mission (Fig. 2.10).

1. Two halves connected at four corners
2. Two halves connected at one point
3. Bottom half deploys drogue

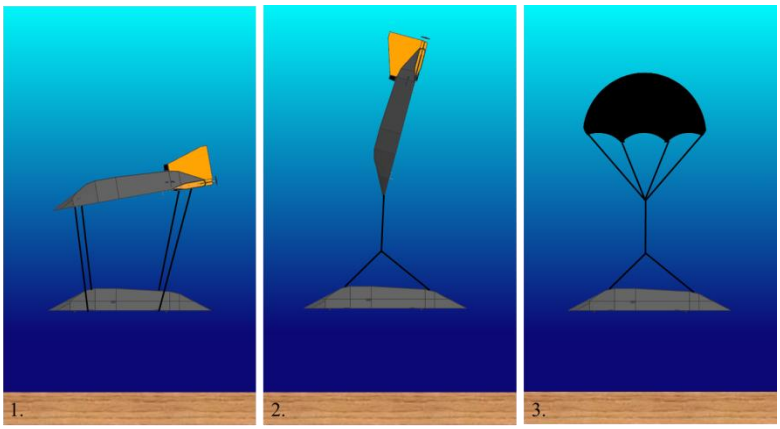

Figure 2.10 Conceptual descent options.

It proved very difficult to accurately simulate the separation, descent and landing to compare these configurations. Specifically, how the two halves will behave after separation and how the linked halves will continue descent. To determine the best option, a scale model was built. The design and testing of this model is described in Chapter 3.

2.2.4 Egress Vehicle Release

After a predetermined amount of time on the seafloor, the inverted half of the ingress vehicle must release the egress vehicle. This operation begins with separation of the top cap to expose the egress vehicle (Fig. 2.11). Buoyant force was determined to be a simple and effective method for releasing both the top cap of the mooring package and the egress vehicle from the mooring package. The top cap must be attached firmly enough to survive impact by trawl equipment during the moored phase of the mission. It must also be effectively released to allow the egress vehicle to exit the mooring mount. The electrical connection between the egress vehicle and the bottom mount must also be disconnected. Both of these mechanisms will be located in the bottom mount which will remain on the seafloor and is a single use system. Because the seafloor mount system is designed as a disposable piece of hardware, it was important to keep cost for this assembly to a minimum. Simplicity and reliability were also important to decrease the chance of failure and reduce the number of design modifications for the egress vehicle nose [7].

The VT-SMAUV utilizes a galvanic release to severe the connection to the vehicle nose anchor. This was a proven method, which could be incorporated into the release design of the bottom

mount top cap. The top cap will be connected to the bottom mount using several latches. These latches will mate with removable pins in the bottom mount. Each pin is connected to a spring held in tension by a fixed cable. A galvanic release will be positioned on a separate cable holding the spring in tension. By activating the galvanic release the cable can be severed, this will allow the spring to pull the pin from the latch disconnecting the top cap. A large amount of positive buoyancy will be located in the top cap. After the latch and pin assembly is disconnected this buoyancy will cause the top cap to lift off the bottom mount and drift free.

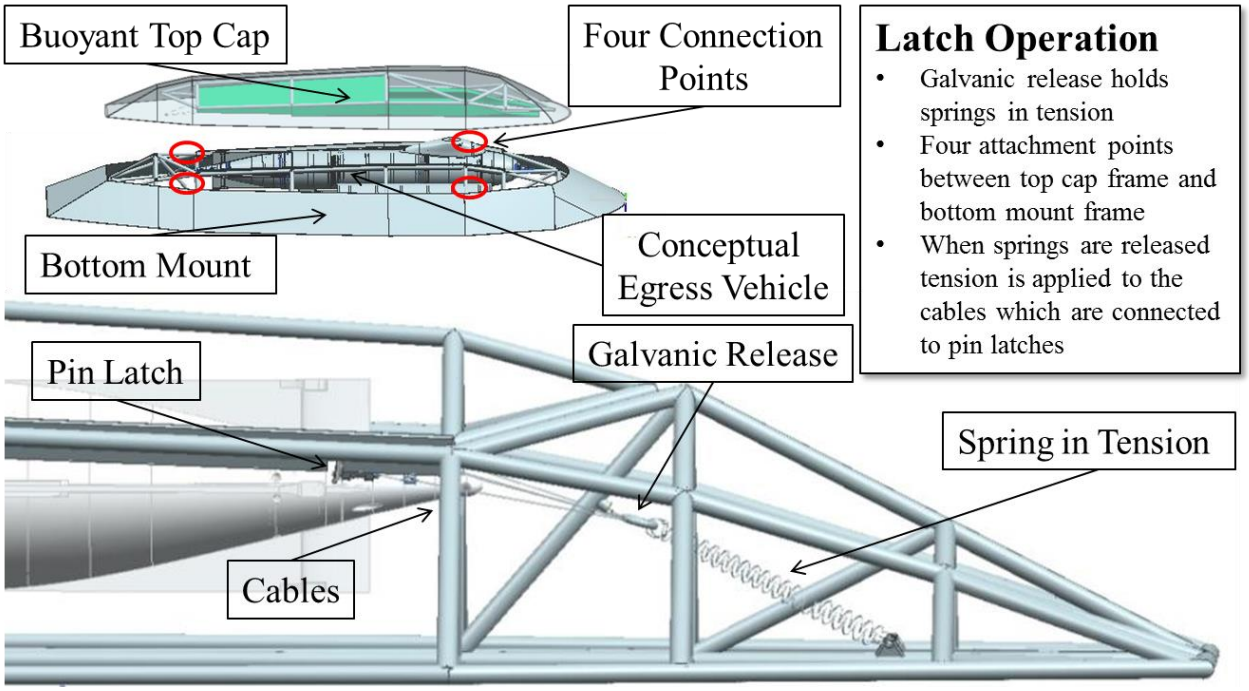

Figure 2.11 Mooring package top cap release [7]

The egress vehicle operates in a slightly positive buoyant configuration. This buoyancy will allow the egress vehicle to drift out of the bottom mount. The last remaining connection to the bottom mount is the electrical cable. Two options were considered to disconnect this electrical umbilical.

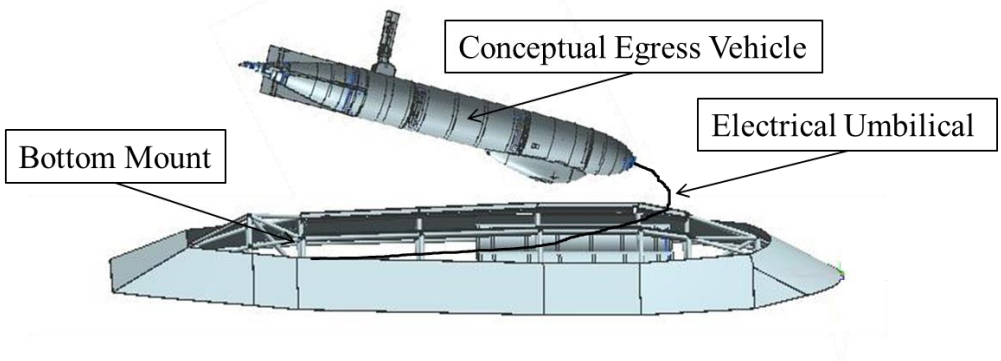

Figure 2.12 Egress vehicle release [7]

1. Pneumatic release: Modification of the internal pneumatic system in the nose of the VT-SMAUV could be used to disconnect two submersible connectors (Fig. 2.13). This modification would enable the pneumatic system to apply a force between the nose mounted bulkhead connector and the mated inline connector. It was estimated that 2000 N of force could be generated at a depth of 500 m.

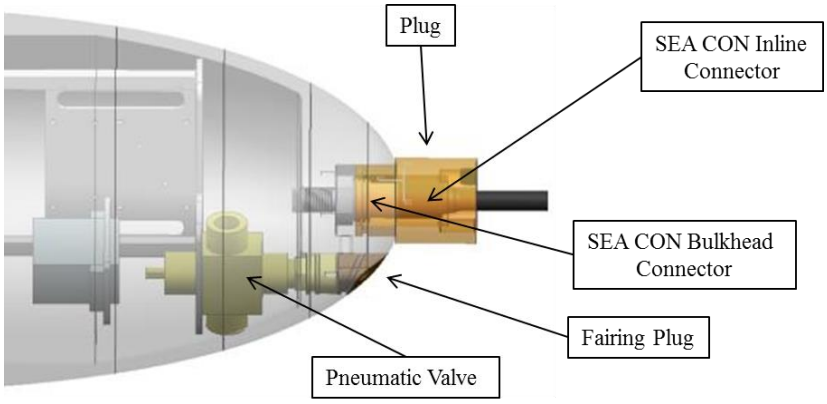

Figure 2.13 Pneumatic release [7]

2. Pyrotechnic release: A pyrotechnic cable cutter could sever the submersible cable. This design would use a fixed bulkhead penetration located in a flat nose bulkhead. A pyrotechnic cable cutter could be used to cut the submersible cable extruding from this penetration. To maintain the hydrodynamic profile a removable fairing would be placed over the flat nose bulkhead.

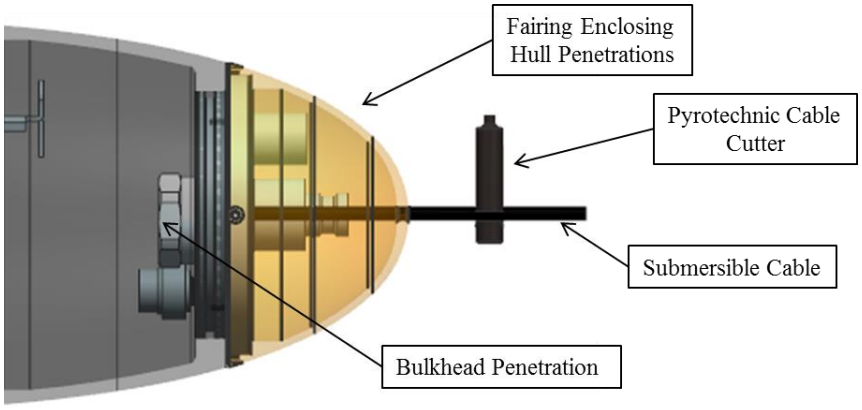

Figure 2.14 Pyrotechnic release [7]

The pyrotechnic release (Fig. 2.14) was selected. It was estimated that this mechanism was more cost effective and also more reliable than the pneumatic release (Fig. 2.13).

3 Ingress Scale Model

A 1/6 size full-scale plastic model of the ingress vehicle was designed and built to validate some of the novel concepts employed in the TRSMAUV. Several of the actions that need to be successfully executed by the ingress vehicle proved very difficult to accurately model. For example, it was very difficult to accurately simulate the behavior of the two halves of the ingress vehicle immediately after separation. Assessing the various passive descent and landing configurations was the primary goal of the TRSMAUV modeling exercise (Fig. 3.1).

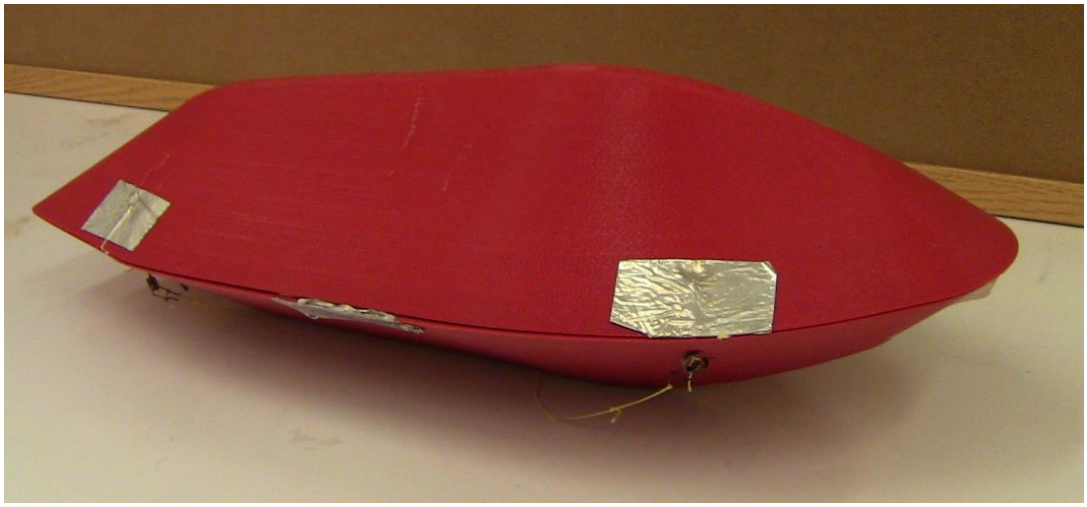

Figure 3.1 TRSMAUV scale model in deployment configuration.

3.1 Design Features

The 1/6 scale TRSMAUV model was designed to be inexpensive and easy to handle. It utilized the shell design presented earlier (Section 2.2.2.1) and was ballasted proportionally to the desired buoyant state of the TRSMAUV immediately prior to separation. The unconventional shape of the TRSMAUV shell, required that the model be fabricated out of ABS plastic using 3-D printing. The scale was determined as the largest size that could be printed with readily available 3D printers. Foam sections and weights were distributed within the hull to correctly ballast the model. The shell was designed with mounting points for testing several different passive descent and landing configurations.

3.2 Testing

Objectives of the model phase of the project were to evaluate the three descent concepts (Section 2.2.3.4) and select the most suitable descent strategy to develop. To achieve a successful landing in the descent phase of the mission several things needed to happen:

1. **Successful Separation:** The bottom half of the ingress vehicle must roll into an inverted position. This maneuver would be accomplished as a result of weight distribution and the mooring configuration (three variations described in Section 2.2.3.4).
2. **Soft Landing:** The bottom half of the ingress vehicle must descend to the seafloor and land without sustaining damage.
3. **Land within CEP:** The two halves must land close to the targeted site following the descent/separation stages.

Model test results were used to determine which conceptual mooring configuration was most likely to be successful. The three configurations described in Section 2.2.3.4 were tested. Multiple tests were performed following a simple procedure.

1. The two halves were attached using the selected configuration
2. The two halves were held in the deployment state midway in the water column
3. The two halves were released and the ensuing separation and landing was observed

Each configuration was tested using different ballast arrangements to optimize the descent and landing phases. Besides evaluating the success in meeting the model test objectives, ease of assembly and ease of integrating the required design specifications into the final vehicle was carefully considered in selecting the design to accomplish the most appropriate descent/landing performance.

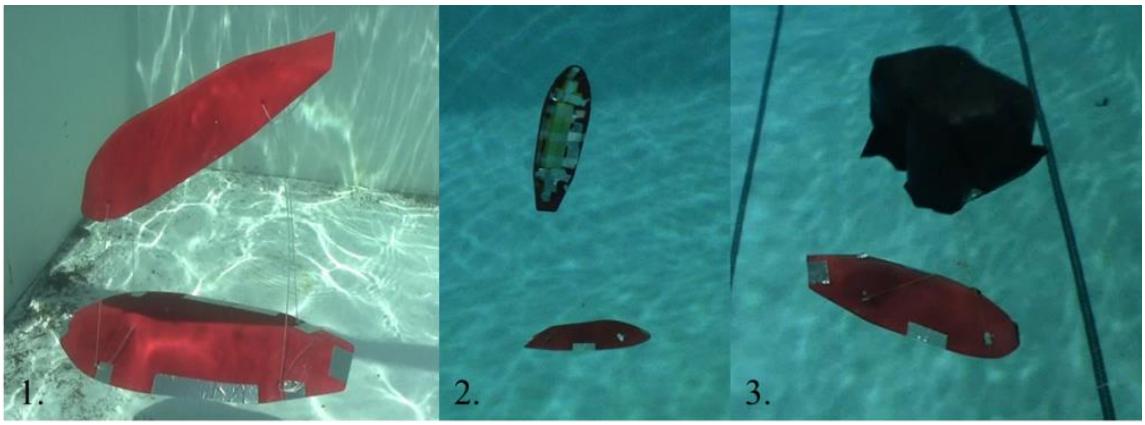

Figure 3.2 The three descent and mooring configurations evaluated during the TRSMAUV scale model tests.

Scale model test results revealed that configuration-2 (two halves connected at one point) was the most effective descent and landing option (Fig. 3.2). Configuration-1 (two halves connected at four points) produced a troublesome gliding effect during descent. This increased the difficulty in predicting where the bottom half would land, thus negatively affecting the desired CEP. Configuration-3 (bottom half deploys drogue) did not yield any visible benefit over configuration-2 while adding unnecessary complications and points of failure.

Further testing was conducted using configuration-2 to determine the optimal bridle and tether design, validate selected locations of center of gravity (CG) and center of buoyancy (CB), and validate selected weight/buoyancy of the two halves. The shortest bridle and tether combination led to the most consistent descent and landing. The overall bridle and tether length was 37.5% of the length of the body. Positions for CG and CB are expressed as ratios of height, width and length of the full size ingress vehicle (Table 3.1). The origin was placed at the midpoint (both vertically and horizontally) of the ingress vehicle leading edge (Fig. 3.3). The vehicle is in a negatively buoyant state immediately prior to separation. This stage occurs after the buoyancy release and helical descent phases of the mission.

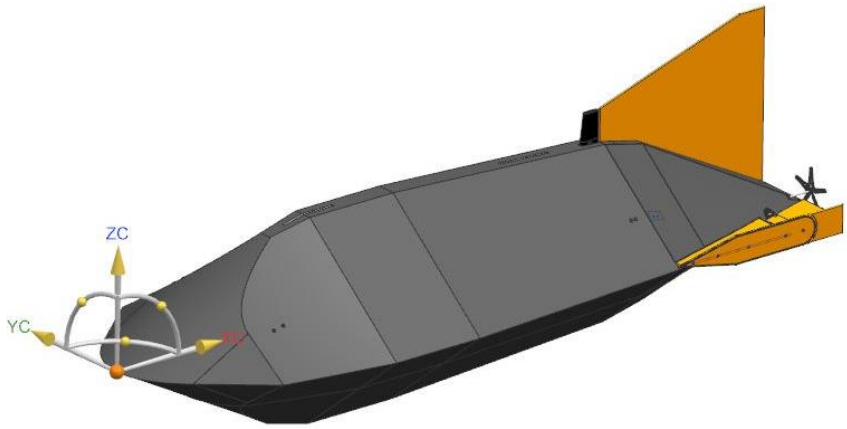

Figure 3.3 Ingress vehicle orientation for trim and ballast calculations

Table 3.1 Weights and CG/CB locations for the ingress vehicle immediately prior to separation [7]

Configuration	CG Position			CB Position			Buoyancy
	X	Y	Z	X	Y	Z	
Ingress Vehicle	0.495	0.000	-0.013	0.501	0.000	0.128	-8%
Bottom Half (Mooring Mount)	0.491	0.000	-0.213	0.491	0.000	-0.286	-110 lbs (for full size vehicle)
Top Half	0.503	0.000	0.348	0.507	0.000	0.381	80 lbs (for full size vehicle)

4 Ingress Limited Prototype

Some of the novel concepts used in the TRSMAUV could not be adequately tested using the scale model. Thus, a limited capability, full size prototype was developed for further testing. This prototype would validate the trawl-resistant capability of the bottom half mooring package, the latch separation mechanism (Section 2.2.3.3), and the full scale passive mooring.

To obtain valid data from field trials with this prototype, the external shape and overall weight distribution was designed to be consistent with the final TRSMAUV. Thus, the shell was fabricated with all the final vehicle capabilities considered. This prototype would lack many of the sub systems used in the final TRSMAUV. The systems that do exist in this prototype were designed so that minimal changes would be necessary to adjust them for final vehicle integration.

Figure 4.1 Limited prototype ingress vehicle being deployed in the Gulf of Mexico

4.1 Shell

The limited prototype shell was designed to the full-scale design specifications described in Section 2.2.2.1. The shell was constructed using a fiberglass layup technique. Fiberglass was selected because it can provide high strength with minimal weight. The layup technique also allows for precise customization of the shell's internal composition so priority can be given to

strength or weight. This was beneficial as it allowed for customization between the top and bottom halves of the shell. The top half was fabricated to minimize wet weight, effectively maximizing the buoyancy. This half only requires enough strength to maintain its shape during flight. The bottom half shell was fabricated to maximize strength with little concern for weight. This half must be strong enough to meet the trawl-resistant specifications.

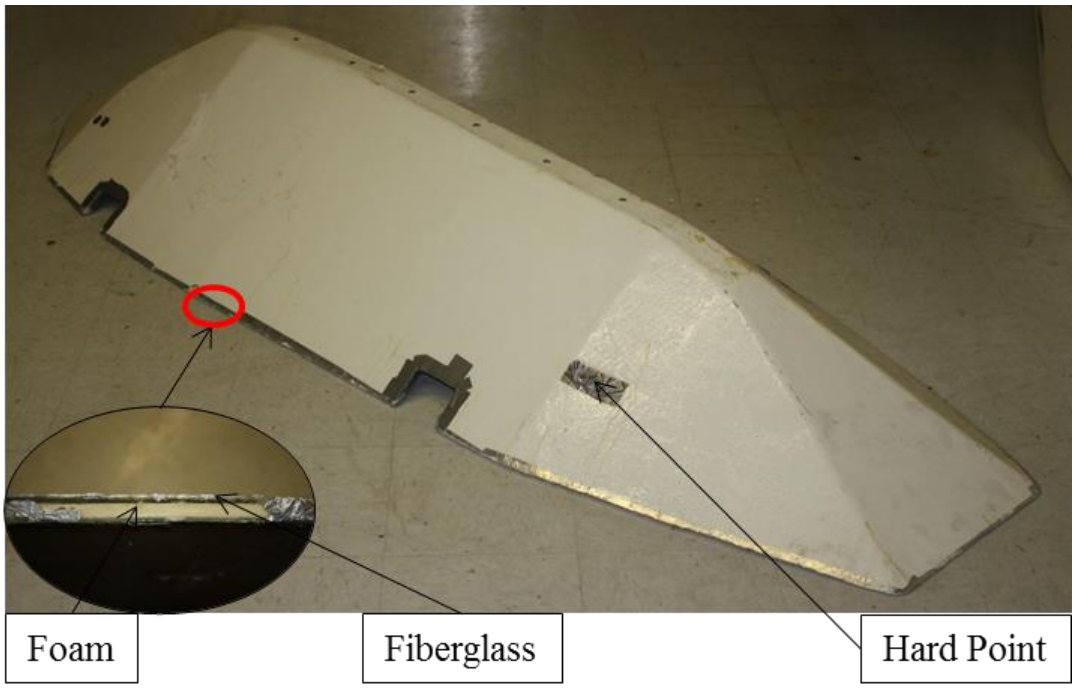

Figure 4.2 Top half shell

The layup process was completed by the design team at Virginia Tech, which greatly reduced fabrication costs. Each shell was fabricated by sandwiching layers of foam between layers of fiberglass (Fig. 4.2). The internal foam adds rigidity and buoyancy to the shell. Four cut outs were positioned along the sides of each shell. These cutouts allowed access to four hoist points, mounted to the internal frame and used for launch and recovery of the prototype. Additional four hard points where added to each shell. These hard points provided mounting points for attaching the shell to the internal frame. The composition of the shell at the hard point location is solid fiberglass. This is important so that holes drilled through the shell do not create a path for water to reach the internal foam. The edge of the shell was sealed with an epoxy resin after the layup process. This ensured that the internal foam could not be exposed to water. If the foam becomes waterlogged it will lose its buoyancy and become immensely heavy.

4.2 Separation

The mechanism to separate the two halves of the limited prototype was based on the rotary latch conceptual design. Four identical servo and latch assemblies were used to fasten the top frame to the bottom frame. These separation assemblies were placed near the corners of the framing to evenly distribute the load. Each assembly was composed of a rotary latch linked to a servo (in a water tight housing). The latch secures to a horizontal pin fixed to the opposite frame.

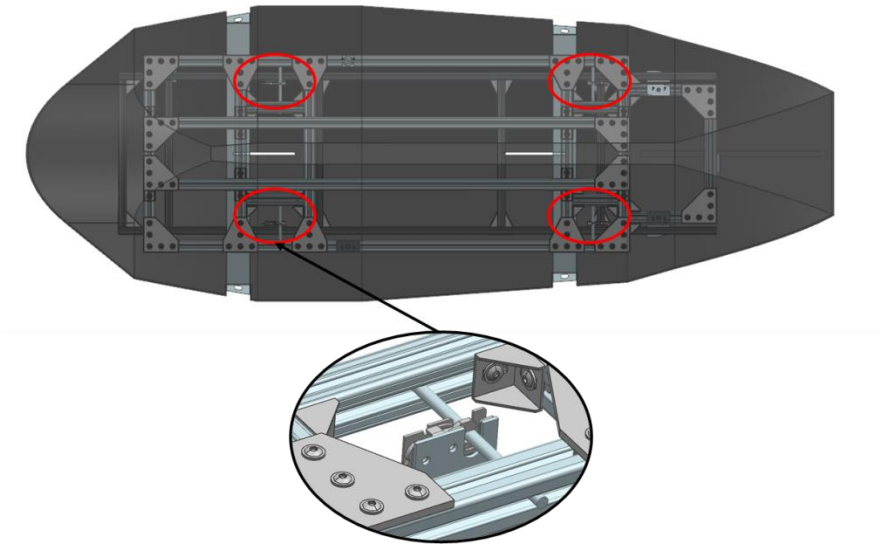

Figure 4.3 Separation layout (S. Portner)

The servo and latch portion of the separation assembly were fixed to the top frame. This is because the other electronics in this prototype are located in the top half shell. By placing the actuating portion of the separation mechanism in the top half, no electrical connections had to be severed. All four servos are simultaneously actuated to open the corresponding latches and release the bottom half to complete the separation phase.

4.3 Mooring

Based on the successful scale model tests, the configuration where two halves were connected at one point was used for the limited prototype. The bridle and tether assembly was designed to be 37.5% of the total body length of the prototype based on scale model tests. Nylon cord was used

for the bridle and tether for the tests. The release of the top half after successful landing was not tested.

4.4 General Assembly

The overall weight of the limited prototype is determined by the wet weight of the mooring package (mooring pressure set at 0.03 psi). The overall buoyant state for this prototype must match what is required immediately prior to separation for valid tests. Ballast was arranged so that the CG and CB closely matched the most successful scale model tests.

The internal framing of both the top and bottom halves was constructed from Aluminum T-slotted framing. The bottom half framing was built from 1.5" solid framing to reduce the amount of additional ballast required. The top half framing was built from 1" framing to minimize the weight and reduce the amount of added buoyancy that would be required. Using Aluminum T-slotted framing was desirable because it reduced the number of custom parts. Large quantities of custom parts can be costly and lengthy to produce. By using off the shelf hardware whenever possible the cost of the limited prototype was reduced. The frames can be easily modified using off the shelf mounting hardware. Likewise, the various subsystems of the vehicle can easily be secured to various points on the frame.

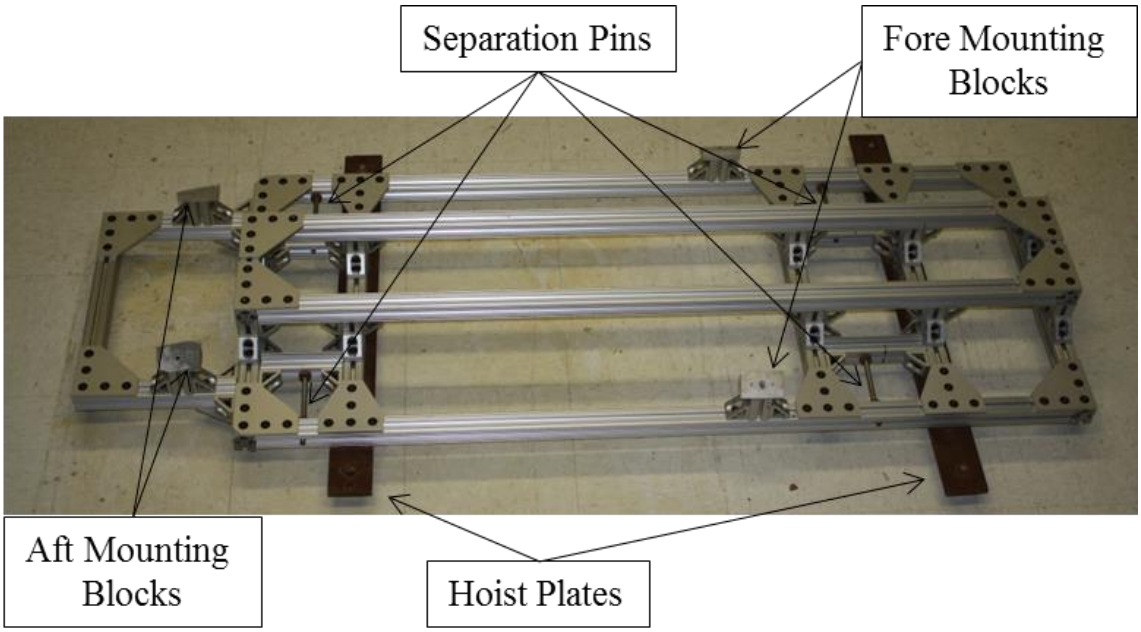

Figure 4.4 Limited prototype bottom frame

4.5 Field Test

The limited prototype field tests were largely successful. Separation of the two halves using the servo actuated rotary latches was unsuccessful. The load applied to the rotary latches was too much for the servos to overcome. Instead, the two halves were held in a temporary state of attachment at the surface, held afloat by a line fixed to the boat. Divers used a quick release on the line to initiate separation. This procedure enabled realistic simulation tests to be conducted of the mooring phase of the ingress vehicle prototype. Test results demonstrated that following separation, the bottom half consistently inverted and performed a slow descent coming to a soft landing on target.

Figure 4.5 Ingress limited prototype separation test

A large chain, with a variety of weights attached to it, was dragged across the deployed mount at an estimated speed of 4 kts to test the trawl-resistant capability of the mooring package. The package successfully deflected the chain without sustaining damage and without a significant change in its moored location through several trials.

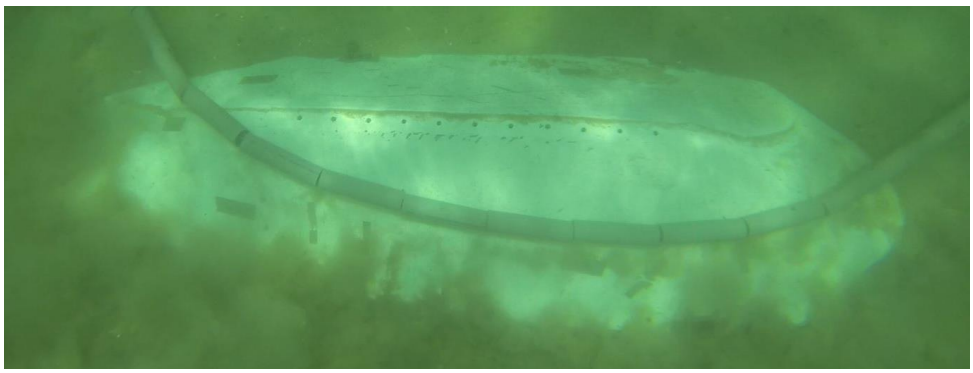

Figure 4.6 Ingress limited prototype trawl resistance test

5 Egress Vehicle

A prototype egress vehicle was unnecessary as the design is nearly identical to the VT-SMAUV. The vehicle nose was modified to incorporate the electrical connection to the ingress vehicle. The external profile of the nose was not altered. This would allow the egress vehicle to use very similar control algorithms to those used in the VT-SMAUV. Another modification reduced the battery pack used in the VT-SMAUV. The egress vehicle only requires power for the fifty nautical mile egress phase of the TRSMAUV mission. Externally, this modification reduced the overall length of the vehicle. New batteries, with a higher energy density (191 Wh/kg vs. 179 Wh/kg), were selected that led to a minor modification in the internal mounting configuration.

Figure 5.1 Field testing the egress vehicle in Claytor Lake, VA

Table 5.1 Egress vehicle specifications

Parameter	Specification
Vehicle Diameter	17.53 cm (6.9 in)
Vehicle Length	1.54 m (60.9 in)
Weight in Air	27.5 kg (60.6 lbs)
Maximum Depth	500 m (1600 ft)
Operating Depth Energy	710 Wh
Endurance	10 – 16 hours (depending on operating speed) Provided by two LiPo 16,000 6S 22.2v battery packs
Propulsion	Direct drive DC brushless motor to open 3-bladed propeller
Velocity Range	Operating speed 2 m/s (3.88 knots)
External Hook-Up	Ethernet and power Cable
Navigation	Attitude Heading and Reference System (AHRS), depth sensor, and GPS
Tracking	Acoustic pinger
CPU/Software	1.7 GHz quad-core Hardkernel ODROID-U3 with a Gentoo OS

5.1 Nose Modifications

Two different conceptual designs were developed to disconnect the electrical connection between the egress vehicle and the ingress vehicle (Section 2.2.4): A pneumatic release and a pyrotechnic release. The pyrotechnic release was selected for use in the final egress vehicle. This mechanism was chosen as it is a simple and very reliable release, which reduced the complexity of the required nose modifications. Electronic wire cutters were selected. These cutters could be activated underwater and have a near perfect success rate.

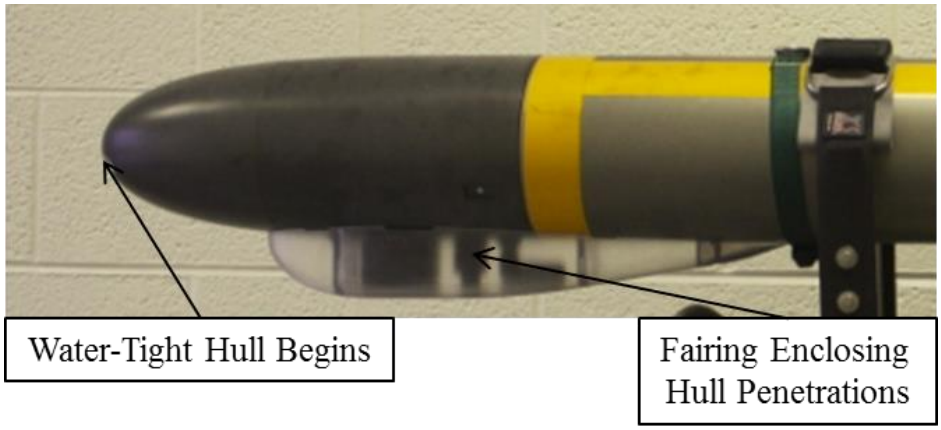

Figure 5.2 VT-SMAUV Nose

The egress vehicle nose was redesigned so that a section of the water-tight hull has a flat bulkhead. This was done so all hull penetrations could be moved to this bulkhead. A removable plastic conical fairing was designed to be positioned over this bulkhead to replicate the external profile of the VT-SMAUV. By relocating the hull penetrations to this nose bulkhead, the fairing located underneath the nose of the VT-SMAUV could be entirely removed. This reduces drag and increases the overall efficiency of the vehicle. A small hole is positioned in the center of the nose fairing for the electrical umbilical to pass through (Fig. 5.3).

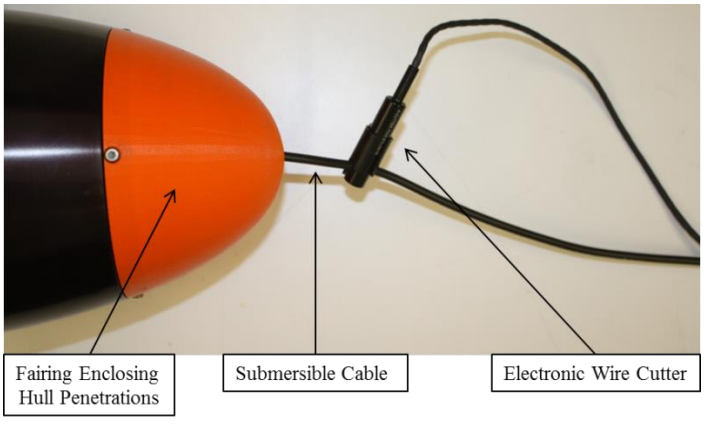

Figure 5.3 Egress vehicle nose

A second depth sensor was added to the nose. The original depth sensor in the VT-SMAUV is located in the tail bulkhead between the oil filled tail section and the air filled tube section of the vehicle. The addition of the second depth sensor gives the egress vehicle the ability to monitor the oil pressure in the tail section. The vacuum valve assembly on the VT-SMAUV was also replaced with a more convenient and lower profile configuration.

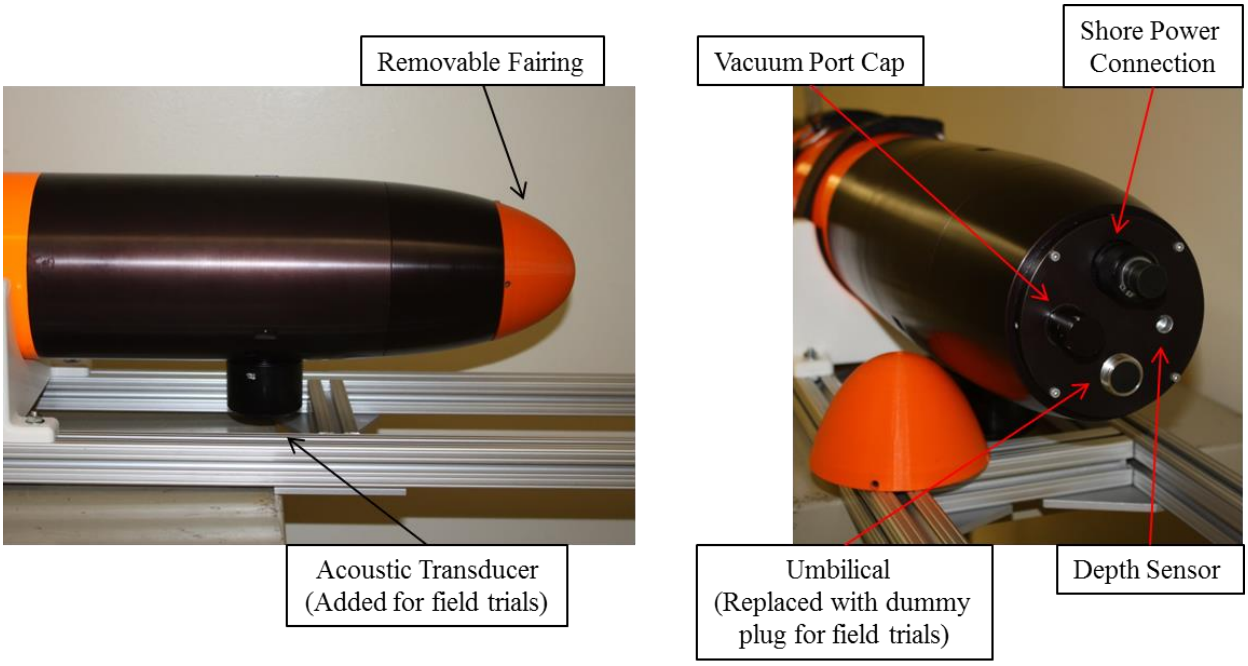

Figure 5.4 Egress vehicle nose shown in the configuration for independent field trials.

The egress vehicle nose is configured for independent operation (Fig. 5.4) or for subsequent tests with the ingress vehicle. A 903 series Teledyne Benthos transducer is installed beneath the nose in this configuration. This acoustic modem uses low and mid frequency ranges for underwater communication during the independent egress vehicle tests. The umbilical bulkhead connector has been replaced with a dummy plug for testing so there are no loose wires.

5.2 Tube Modifications

The middle section of the egress vehicle was modified from the VT-SMAUV design. The battery pack required by the egress vehicle is much smaller than the pack in the VT-SMAUV. This reduction in size reduced the length of the middle section of the egress vehicle. The VT-SMAUV middle section comprises several 10 inch long tube sections. Each tube section connection adds another seam that can become damaged and lead to a loss of water-tight integrity. These short tube sections were replaced with a single 17” long tube in the egress vehicle. This change reduced the length of the egress vehicle by 13” to 61” overall.

5.3 Field Testing

Initial testing of the egress vehicle was performed using the control algorithm from the VT-SMAUV. The general characteristics of the egress vehicle are very similar to the VT-SMAUV so it was estimated that few changes, if any, would be required to the controller. Preliminary testing was carried out in Claytor Lake, VA and final mission testing will take place in the Gulf of Mexico, near Panama City Beach, FL. To test the effectiveness of the controller, a series of missions were executed to excite the dynamics of the vehicle. These missions included flights stepping between different heading commands (yaw steps mission) and flights stepping between different depth commands (depth steps mission). The egress vehicle demonstrated adequate control through both the yaw steps missions (Fig 5.5) and the depth steps missions (Fig. 5.6 & Fig. 5.7). The egress vehicle repeatedly reached commanded headings and depths efficiently with minimal overshoot.

The egress vehicle experienced significant roll perturbations during the yaw steps mission (Fig. 5.5). This was most likely due to the drag effects generated by the static mast when the vehicle was at a large side slip angle. The roll is larger than what the VT-SMAUV experienced during similar maneuvers. This is because the egress vehicle body is shorter and responds more aggressively to control surface deflections thereby inducing more side-slip than the VT-SMAUV.

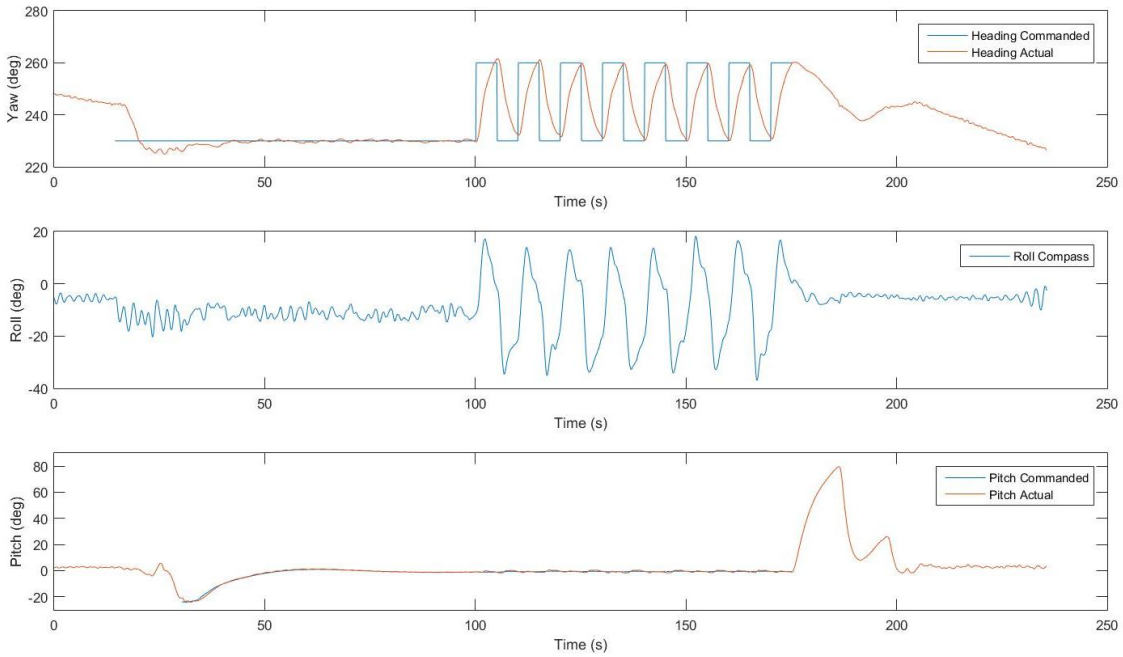

Figure 5.5 Egress vehicle yaw steps mission (Euler angles)

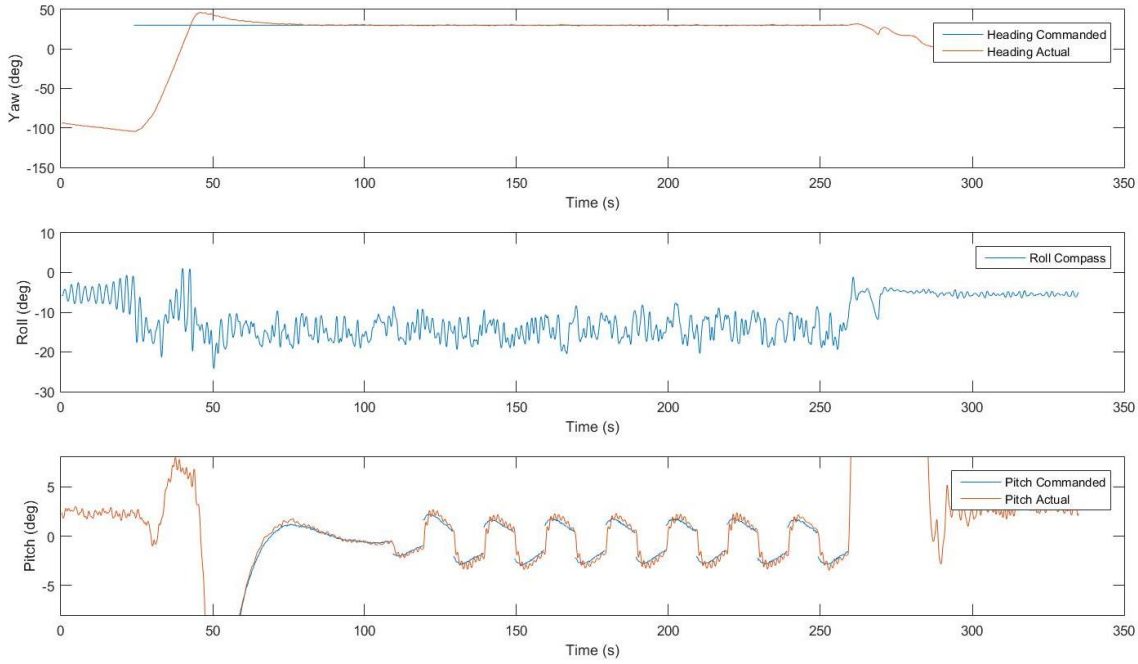

Figure 5.6 Egress vehicle depth steps mission (Euler angles)

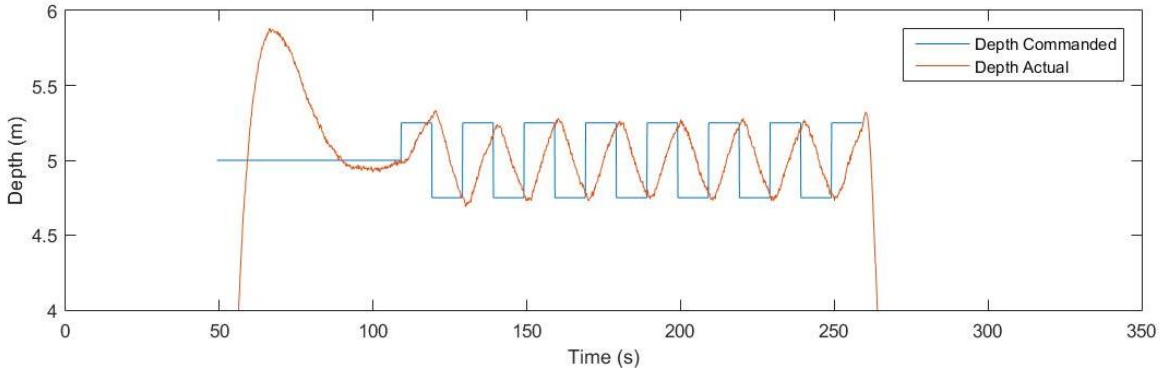

Figure 5.7 Egress vehicle depth steps mission (depth)

The VT-SMAUV controller proved to be satisfactory for egress vehicle operation. However, a new, more appropriate, controller is in development and will be tuned with further field testing.

6 Ingress Vehicle Prototype

A final prototype ingress vehicle was designed and built to test the flight ability, buoyancy release, helical descent, separation and landing after successful validation of the full scale novel concepts used in the TRSMAUV (Chapter 4). The internal layout of this prototype's sub systems is nearly identical to the final TRSMAUV. Although this prototype was designed with space to house the egress vehicle, it does not contain the mounting or release hardware.

6.1 Stability

The unusual shape of the TRSMAUV ingress vehicle presented many stability problems. Vehicle stability can be decomposed into three important dimensions: pitch, roll and yaw. Stability can be further decomposed into two different states: static (the vehicle is not moving), and dynamic (the vehicle is moving). Static yaw stability is not a concern because the TRSMAUV is only required to maintain a specific yaw heading while moving.

In a static state, only pitch and roll stability were addressed. In a dynamic state, stability is required in all three dimensions (pitch, yaw and roll). Dynamic stability is required for efficient controlled flight. While moving, the hydrodynamic forces experienced in the yaw and roll dimensions are relatively small, because of this, passive dynamic stability can be achieved. Dynamic stability in pitch is more difficult due to the large hydrodynamic forces experienced while underway. This vehicle utilizes different mechanical systems to achieve active dynamic stability in pitch (Section 6.3).

Static stability in pitch and roll can be obtained in marine vehicles by the correct placement of vehicle CG and CB. A large vertical separation between the CG and CB leads to good static stability in pitch and roll. While underway hydrodynamic forces affecting roll are minimal, thus dynamic stability in roll can also be gained from the placement of CG and CB. The longitudinal and latitudinal positions of the CB and CG are also important. Inconsistencies in this placement can lead to undesirable vehicle list or trim. The ingress vehicle design placed the heavy bottom half mooring package underneath the buoyant top half creating a significant separation between CB and CG. This provided static stability in pitch and both static and dynamic stability in roll without negatively affecting the position of other vehicle subsystems.

A fixed skeg was added to the aft section of the vehicle to achieve sufficient dynamic stability in yaw. The correct sizing of this skeg required a detailed analysis of the hydrodynamic forces experienced by the ingress vehicle with no skeg. A steady CFD analysis was run on the ingress vehicle body at multiple yaw angles of attack (Fig. 6.1) [6].

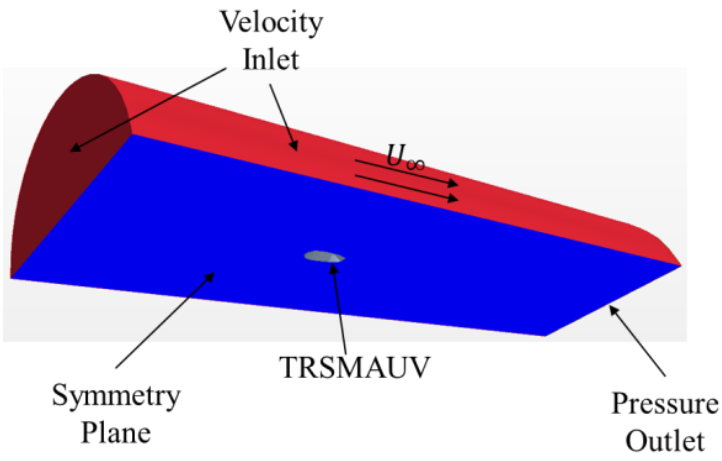

Figure 6.1 CFD simulation set up [6]

The moment experienced by the ingress vehicle could be determined from the simulation results. The skeg must generate enough lift to counteract this moment. The skeg surface area was calculated by approximating the lift generated by the skeg using an ideal 2D airfoil approximation. Initially the skeg height was set equal to the height of the ingress vehicle. This would reduce the risk of damage during transportation. This resulted in a preliminary skeg size of 0.126 m^2 (Fig. 6.2). Another CFD analysis was run to check the accuracy of the ideal 2D approximation.

The CFD simulation showed that the 0.126 m^2 skeg provided only about half the required restoring moment. This was likely a result of the skeg's lack of a leading edge because it is connected directly to the shell (Fig. 6.2). The correct surface area required was determined to be 0.2 m^2 based on further CFD simulations (Fig. 6.3). With this increase in surface area it became impractical to keep the height equal to the ingress vehicle height. Instead, the length was fixed at the trailing edge of the ingress vehicle (Fig. 6.2).

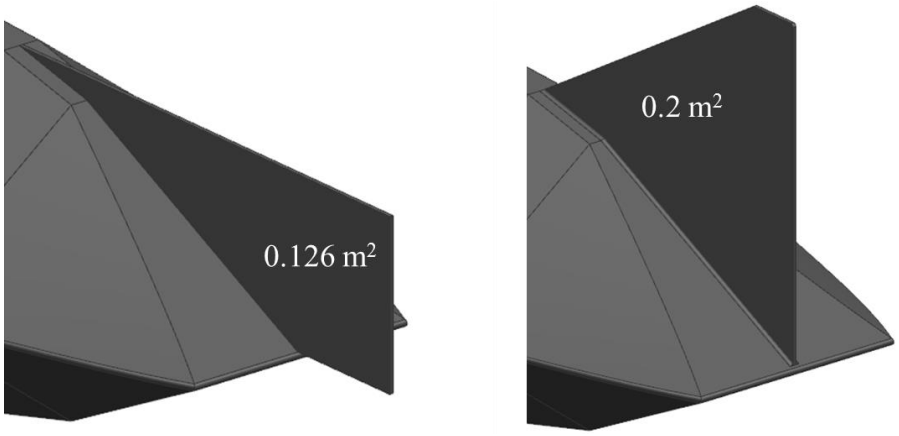

Figure 6.2 Preliminary skeg (left) final skeg (right).

Many uncertainties remained on how the skeg would affect the stability of the ingress vehicle during field trials. For this reason, the skeg was ultimately designed so that it could be easily replaced with alternate skeg designs, if needed.

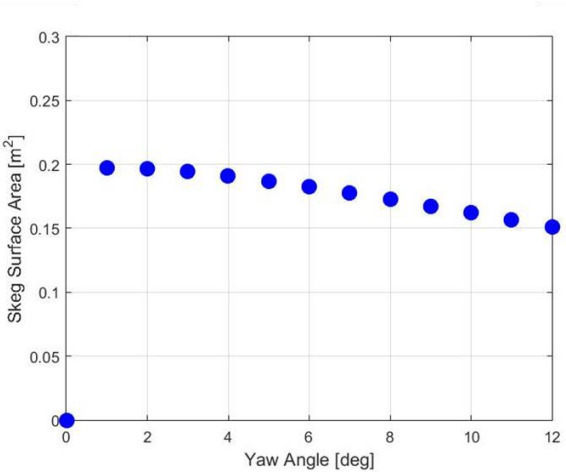

Figure 6.3 Skeg surface area required to produce zero net moment at various yaw angles of attack [6]

6.2 Propulsion

The preliminary CFD analysis (Section 2.2.3.2) resulted in the decision to use a twin screw configuration. This produced a similar efficiency to the single screw system but provided several benefits compared to the single screw configuration. The most important benefit was the ability to control yaw using differential thrust. Further analysis was necessary to determine whether the dual screw optimal configuration was inboard or outboard (completed by E. Ball). Two CAD models that included the final skeg designs and hypothetical elevators for the inboard configuration were used for the CFD analysis (Fig. 6.4).

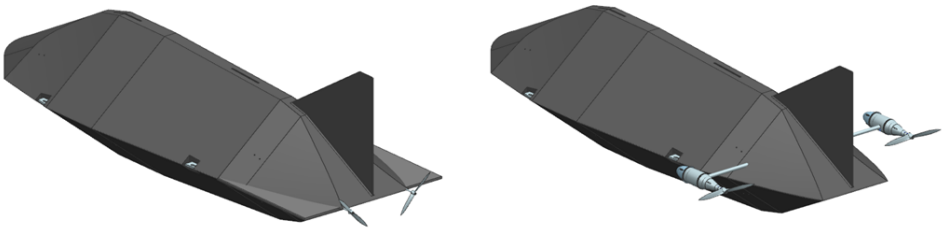

Figure 6.4 CAD models used for CFD analysis showing the inboard (left) and outboard (right) propeller configurations.

A CFD simulation using these CAD models generated more accurate drag estimates than the previous CFD work (Section 2.2.2.2). These simulations also generated velocity inflow profiles for the different propeller positions. The results indicated that the novel shape of the ingress vehicle produced a large wake leading to a non-uniform velocity inflow profile for the inboard propellers (Fig. 6.5).

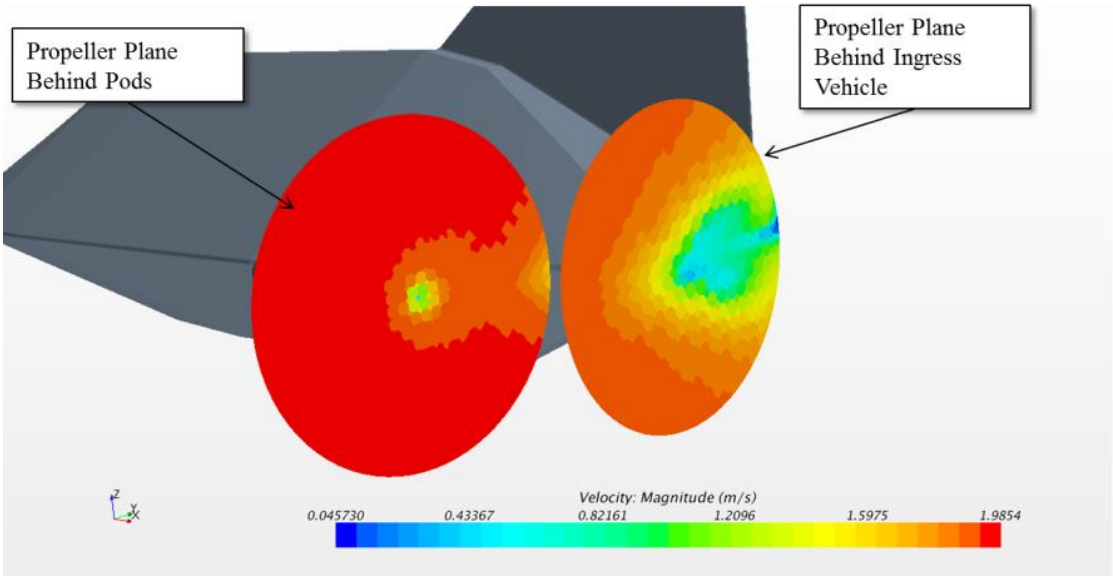

Figure 6.5 Flow velocity profile shown behind the vehicle and behind the motor pod. Note the asymmetry in the flow field associated with the propeller positioned behind the vehicle [6].

The outboard configuration generated more drag but allowed propellers to operate in a consistent flow distribution. The inboard configuration reduced drag but the propellers operated in an inconsistent flow distribution. The area of large velocity deficit in the wake covered approximately 25% of the propeller disk area. To account for the irregular velocity inflow profile, it was estimated that the inboard propellers produced 25% less thrust, due to the blades stalling in this region, than they would if this region were not present. Overall efficiency of each configuration was determined using CFD simulation, OpenProp, and Matlab. The general procedure is outlined below and is the same as the initial propulsion analysis (Section 2.2.3.2).

Inboard vs. Outboard Configuration Selection:

1. Use CFD to determine velocity inflow profile and vehicle drag profile.
2. Use OpenProp to determine torque vs rpm curves for each propeller diameter and number of blades.
3. Use a Matlab script to match each COTS motor with each propeller diameter by finding the intersection of torque vs rpm propeller curve with torque vs rpm motor curves. This is completed over a combination of assumed battery voltage and gear ratios.
4. Calculate overall efficiency of each motor/propeller combination.

The best overall vehicle efficiency was very similar for both configurations. Consideration was given to the mechanical design difficulty of both configurations in making the decision for which design to choose. The inboard configuration was chosen as the outboard design was estimated to be more difficult and more expensive to design and implement. The final phase of the propulsion design stage was to determine an optimal propeller design and pair it with a COTS motor. This was completed using CFD simulation, OpenProp and XFOIL. For both OpenProp and XFOIL, design parameters were selected to optimize the propellers for operation in low Reynolds number ranges. The general procedure is described below.

Propeller Design Optimization:

1. Assume a propeller blade drag profile based on propeller size.
2. Repeat steps 1-3 from the Configuration Selection procedure.
3. Select the optimal COTS motor and propeller pair.
4. Design propeller blades by radial sections based on calculated lift distribution, axial/tangential velocities, and pitch angle.
    i. Calculate lift per unit span based on lift coefficient distribution (determined from circulation distribution).
    ii. Determine chord lengths based on the range of lift coefficients considered.
    iii. Specify thickness distributions.
    iv. Calculate Reynolds numbers at each radial position for each chord length.
    v. Determine the best lift over drag, best camber and best position of max camber for all lift coefficients considered at each station.
    vi. Select the thickness distribution, Reynolds number distribution and lift coefficient distribution at each station that corresponds to the lift coefficient maximizing the lift over drag at each station. This maximizes thrust for a given torque.
    vii. Smooth lift coefficient distribution and repeat steps ii – vi.
    viii. Calculate propeller drag profile and thrust using XFOIL.
5. Check that the propeller drag profile determined in step 4.viii is similar to the drag profile used in step 1. If not, use the updated drag profile and repeat steps 1-4.
6. Check propeller for cavitation in OpenProp and alter lift coefficient distribution if necessary.
7. CAD file is output by OpenProp for rapid prototyping.
8. Use FEA techniques to select a material and manufacturing procedure for propeller.

Table 6.1 Propulsion design specifications [6]

Optimal Diameter (in)	6.5
Optimal Gear Ratio	1
Optimal Peak Voltage (V) (90% duty cycle)	13.32
Optimal Number of Blades	5
Optimal Propeller RPM	1670
Optimal Efficiency	0.42723
Optimal Current Draw (Amps)	10.2594
Optimal Torque on Propeller (N-m)	-0.6397
Optimal Motor	Neumotors 1924/3Y/6MM

The forces experienced by the propeller blades must be examined to select a material for their construction. For low quantities of small, abnormally shaped parts, 3D printing out of ABS plastic is very cost effective. This procedure is commonly used for small propellers because the forces are relatively small and stresses do not exceed material yield strength.

Figure 6.6 Prototype ingress vehicle propeller. ABS (left) Nickel and Copper plated ABS (right)

The propeller blades for the ingress vehicle will be larger and will thus experience forces that may cause significant deformation of ABS plastic. Blade deformation can present problems because the propeller will not operate as designed. This can result in negative effects on the efficiency. Two possible solutions to this problem are: print the propellers out of metal (e.g. stainless steel), or plate plastic propellers with metal (e.g nickel). Printed stainless steel parts will often have a rough finish. This can negatively affect the propeller performance. Plating plastic propellers can lead to similar rough finish issues and may not add the required strength. For this prototype, propellers of several different materials will be field tested to determine the best option.

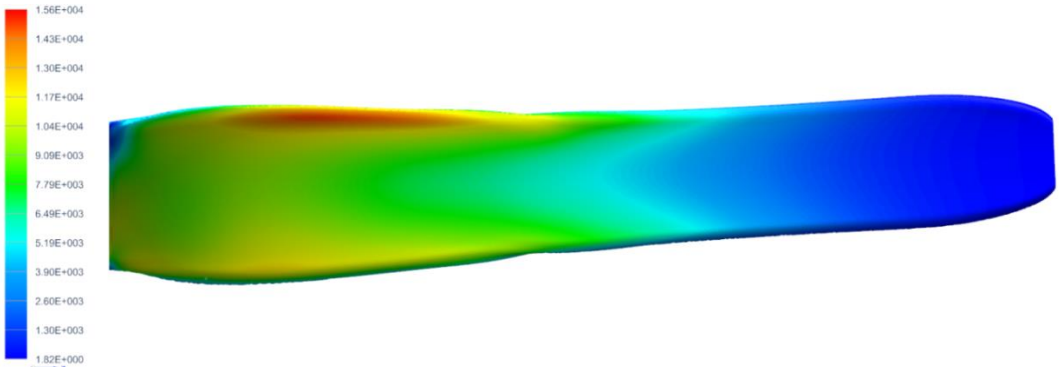

Figure 6.7 FEA results on ABS propeller blade (psi) [6]

The blades of a propeller of this design, fabricated out of ABS, may fail when subject to stresses $\geq 6.16 \times 10^3$ psi (yield strength of ABS). Stresses exceeding this value are indicated by shades of green, yellow, orange and red in the FEA simulation (Fig. 6.7). It should be noted that elastic deformation may occur well before these stresses, and can have an equally negative effect on propeller performance.

A final CFD simulation was performed to ensure that the ingress vehicle could overcome the passive stability generated by the skeg and execute a controlled yaw command. Simulation estimated that the ingress vehicle can adjust course at roughly 0.5 degrees/second (Fig. 6.8). This simulation generated a conservative result because it was run assuming one propeller generating maximum thrust and the other propeller generating zero thrust. Yaw commands could be executed more rapidly by operating propellers in opposite directions at maximum thrust.

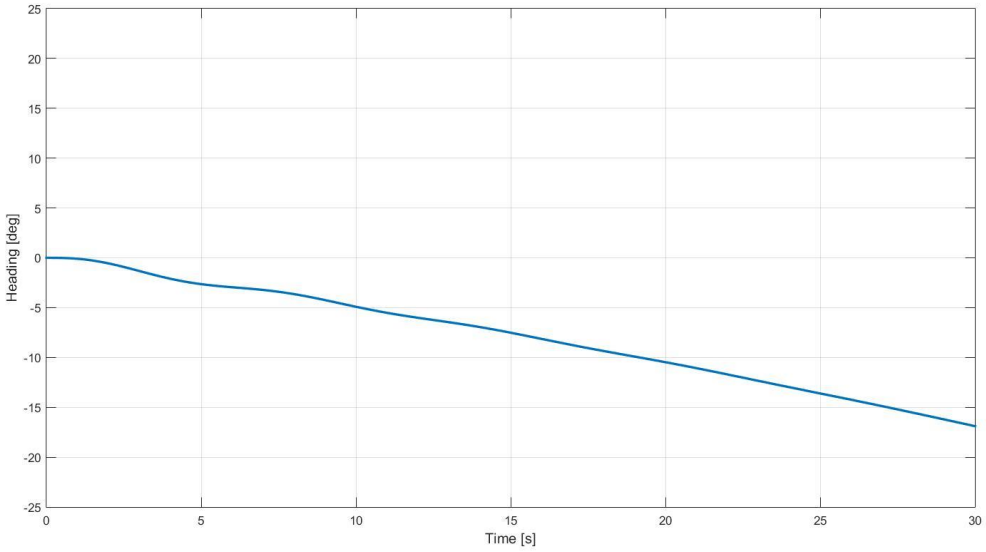

Figure 6.8 Ingress vehicle yaw command from one propeller at maximum thrust [6]

6.3 Dynamic Pitch Stability

The inboard propulsion system eliminated the possibility of pitch control from actuating motor propeller pods. A more conventional elevator design was chosen instead. Pitch control is required to correct pitch perturbations that may occur while the ingress vehicle is underway. The elevators must be able to correct these changes in the angle of attack and keep the vehicle on a level flight path. Additionally the elevators must provide enough moment to initiate a dive.

The ingress vehicle must achieve a slightly negative pitching angle of attack to execute a dive. To accomplish this, the elevator must generate a moment that can overcome the righting moment generated by the body when subjected to a pitching angle of attack. This righting moment is a result of the vertical separation between the vehicle CG and CB. A vehicle of this size will also experience a significant Munk moment when subjected to a nonzero pitch angle of attack. The Munk moment is a result of the hydrodynamic forces and can lead to uncontrollable pitching of the vehicle. The elevators must not only generate a large enough moment to overcome the righting moment, but also must hold the vehicle at the desired angle of attack during the dive. CFD analysis was used to determine the minimum size elevator that is necessary to generate the desired pitch control [6].

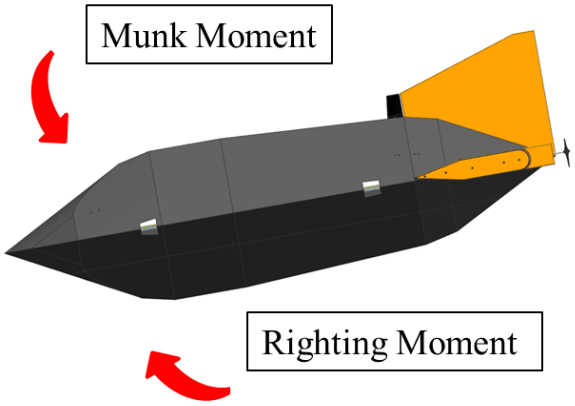

Figure 6.9 Moments experienced by the ingress vehicle at nonzero pitching angles of attack

CFD simulations were run at several different pitch angles of attack to estimate the net moment experienced by the ingress vehicle. From these results an elevator size was estimated. The elevators were designed to be within the maximum width of the ingress vehicle. This reduces the risk of damage when transporting the vehicle. A fixed strake is positioned directly in front of an actuating flap to maximize the moment generated by the elevators. The flap induces a pressure distribution on the strake as well as the flap when it is actuated, increasing the effectiveness of the flap. This elevator assembly was then added to the CAD model and further CFD simulations were run to confirm the elevators could produce the required moment (Fig 6.10).

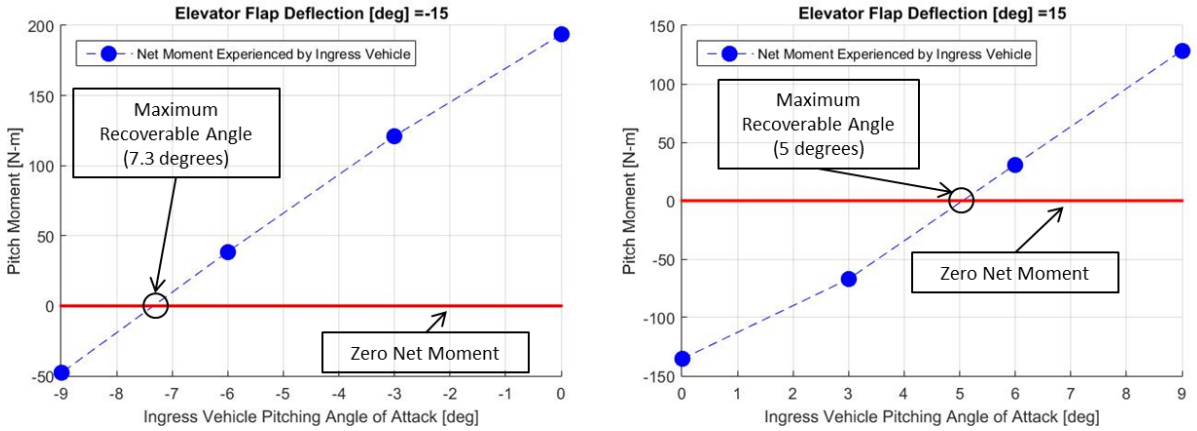

Figure 6.10 Righting moment generated by flaps when deflected at 15 degrees in both directions [6]

The first elevator assembly generated a moment only sufficient to actively control the ingress vehicle at minimal angles of attack (less than one degree in either direction). Vertical plates were added to the ends of the fixed strakes and elevator flaps to make the elevators more effective, without exceeding the maximum width of the vehicle (Fig. 6.11). These plates reduced vortex shedding along the edge of the elevator and increased the lift. This elevator assembly was estimated to be capable of generating a moment that could actively control the ingress vehicle at pitch angles of attack between -7.3 degrees and 5.0 degrees (Fig. 6.10).

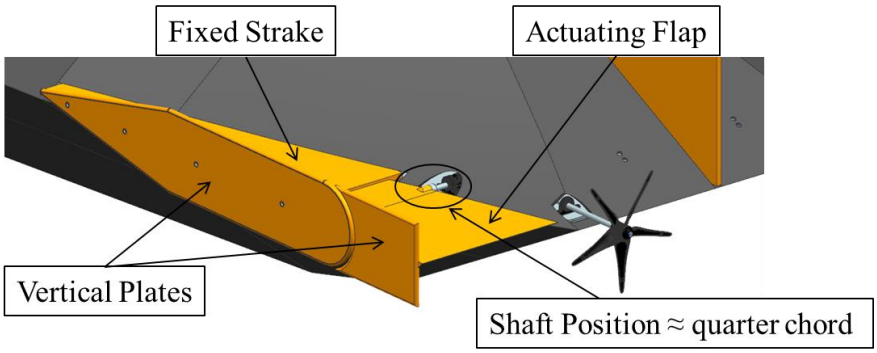

Figure 6.11 Elevator assembly

It was necessary to find a suitable actuator for the flap after sizing the elevator assembly. The flaps were designed using a balanced rudder concept. By placing the shaft at roughly the quarter chord, the torque on the shaft was reduced. The maximum torque that is exerted on the shaft was estimated to be 270 oz-in based on the CFD simulations (Fig 6.12). This value was then used to select a suitable commercially available servo. To account for additional torque from seal losses and provide an acceptable factor of safety (FoS), servos where selected with a maximum torque of 500 oz-in.

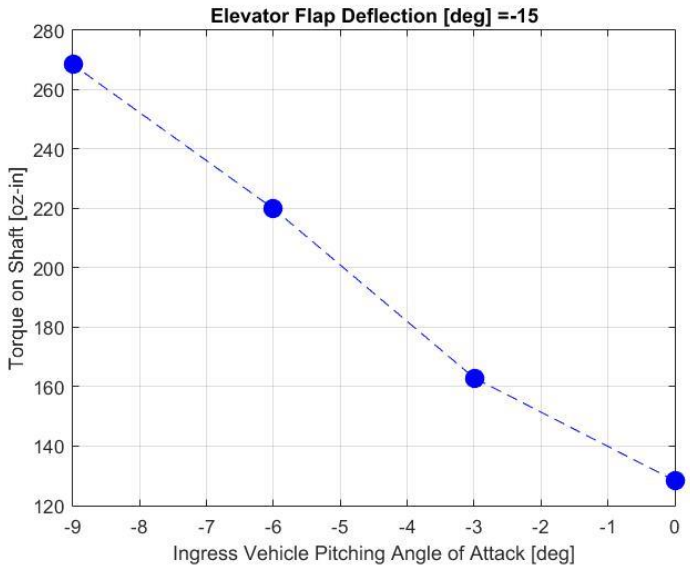

Figure 6.12 Torque experienced by elevator shaft when the flap is at max deflection at various angles of attack [6]

6.4 Buoyancy Control

The ingress vehicle must possess a certain amount of disposable buoyancy as stated earlier (Section 2.2.3.1). The TRSMAUV executes a one-time change of buoyancy immediately before the helical descent. To successfully land on target this buoyancy release must occur rapidly. Buoyancy is supplied from several air tubes in the ingress vehicle. These tubes are designed with ejectable bulkheads for rapid flooding.

Each tube is constructed from lengths of schedule 40 PVC tubing (6" pipe size). The PVC tubing provides a suitably strong pressure housing because this buoyancy is only necessary during the ingress phase of the mission which occurs at shallow depth. Each tube is sealed at both ends by a solid PVC endcap with a gasket (made of soft silicon based rubber) providing a face seal. A high strength compression spring is mounted to an internal ring at each end of the tube and is put into a compressed state while the tube is in its buoyant state. In the buoyant state the two endcaps are held in place by high strength stretch resistant line (Dyneema). To flood the tube this line is cut using the same electronic wire cutters used for the egress vehicle release. The compressed springs provide enough force to overcome the hydrostatic pressure exerted on the endcaps at the cruising depth and thus release the endcaps. The tube, now open at both ends, will flood almost instantaneously.

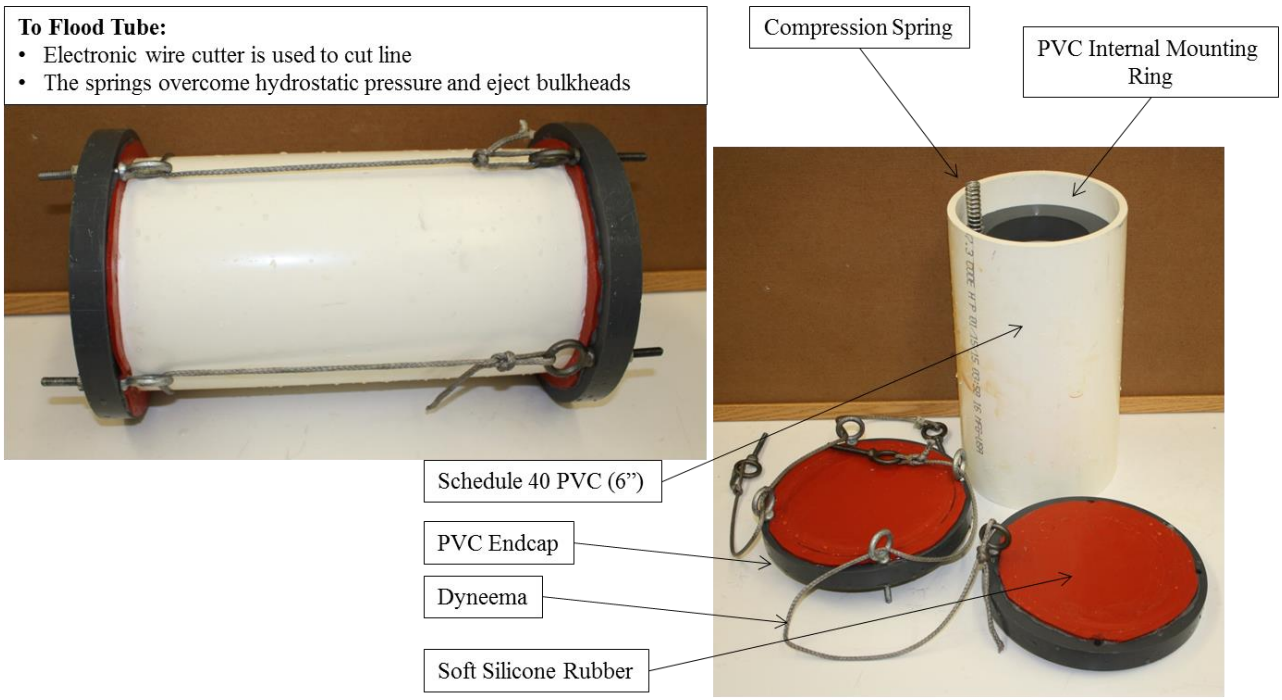

Figure 6.13 Prototype buoyancy tube

6.5 Separation

The limited prototype vehicle demonstrated that the rotary latches were ineffective for separation of the two shell halves (Chapter 4). A separation mechanism was designed using the same electric wire cutters used for buoyancy release and egress vehicle release. Loading between the two halves was broken down into two components to simplify the separation mechanism design (Fig. 6.14):

1. A vertical load composed of: i) a large static load from the buoyancy difference of the two halves, and ii) smaller hydrodynamic forces exerted on the ingress vehicle while underway.
2. A shearing load: The maximum shearing load was considered to be the weight of the top half. This force could result from the vehicle being turned on its side.

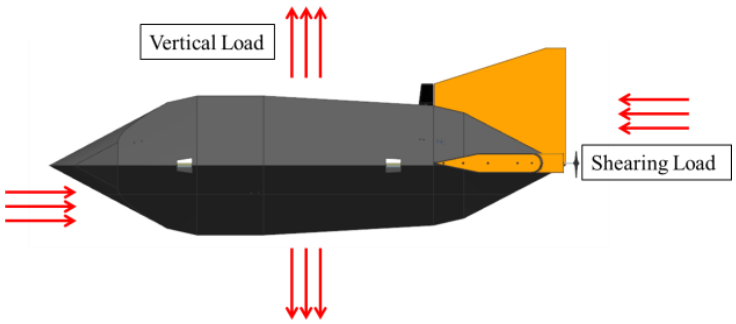

Figure 6.14 General decomposition of loading forces between the two halves

The vertical loading is carried by two steel cables. There are two identical separation cable assemblies located in the ingress vehicle; both are positioned along the centerline, one fore and one aft. Using only one assembly was considered although this could lead to shifting between the two halves during deployment. Having two connection points reduces this risk. Two assemblies also enabled the selection of a lighter steel cable that would be strong enough for the application. Each cable is fitted with stud end fittings. These studs enable preloading of the cables to securely fasten the two halves of the ingress vehicle together for initial deployment of the TRSMAUV (Fig. 6.15). When the TRSMAUV is deployed, it will be hoisted into the water using a sling. This ensures that the cables are never required to support the dry weight of the bottom half.

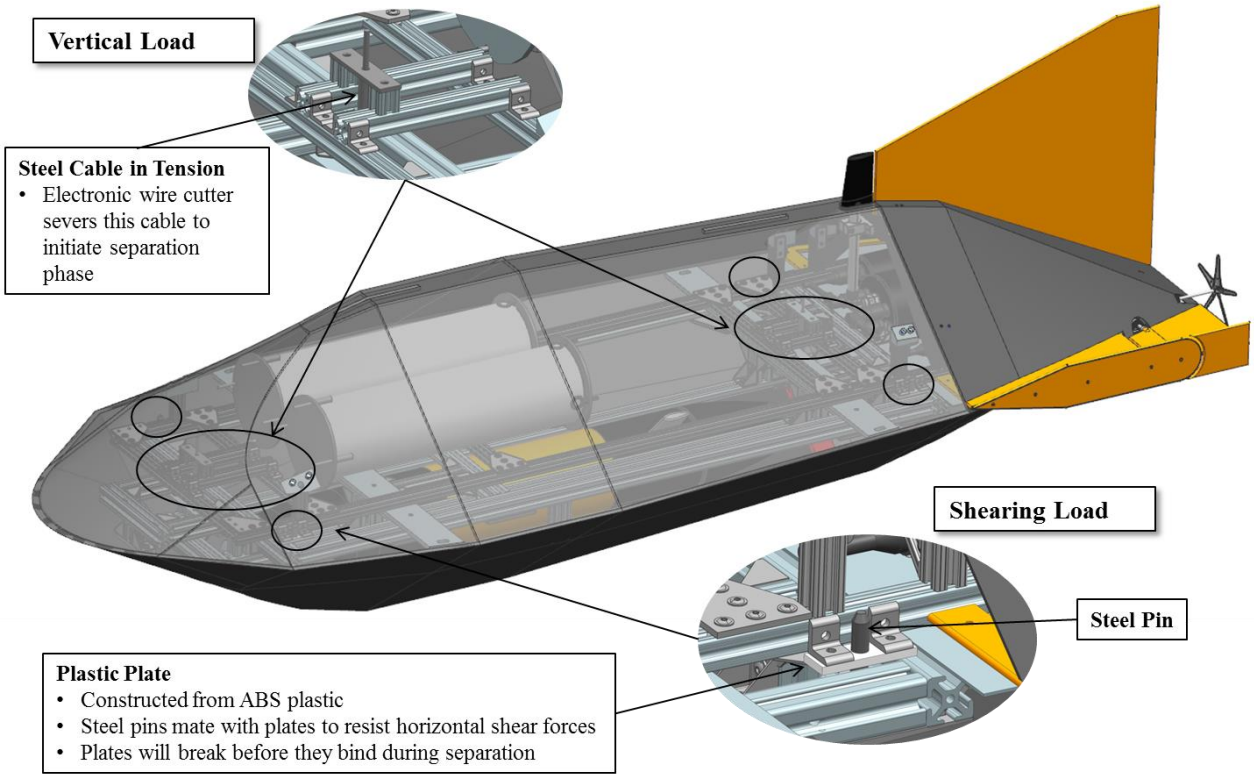

Figure 6.15 Separation assembly placement in the TRSMAUV ingress vehicle, electronic wire cutters sever cable and differential buoyancy between the two vehicle halves causes separation.

To resist the shearing load, four steel pins are mounted at the corners of the bottom half frame. These pins double as locating pins when connecting the top half to the bottom half. Each pin has a heavy chamfer on the tip to help align pin into the mating plate fixed to the top half frame. It is important to consider the risk of the two halves binding on these pins when the vertical connection is severed. To prevent this, the plates are constructed of ABS plastic. The plates are designed to resist the shearing loading while the ingress vehicle is in the deployment configuration. Each of the four plates was designed assuming it would carry $1/4^{th}$ of the shearing load. A 2 mm thickness was selected using a minimal FoS (1.32) based on the highest stress revealed by an FEA simulation; 4.65×10^3 psi (yield strength of ABS taken as 6.16×10^3 psi) (Fig. 6.16). When the vertical connection is severed it was estimated that these plates will be subject to a much higher force and will break before binding. This will be experimentally tested during field trials to find the optimal plate thickness.

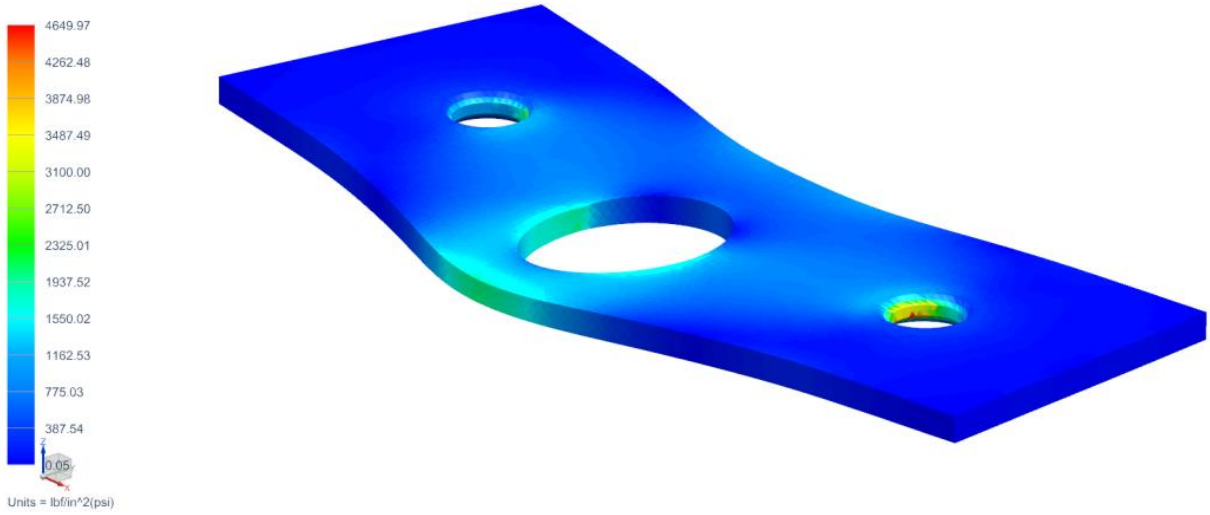

Figure 6.16 Finite Element Analysis (FEA) results on ABS plastic alignment plate.

During the mission the separation phase is initiated by firing the electric wire cutters and cutting the cables. The different buoyant forces of the two halves cause the two halves to separate and begin the mooring phase.

6.6 Pressure Vessels

The ingress vehicle of the TRSMAUV is not designed to be entirely water tight. Many of the components in the vehicle do not need a dry environment to operate. However, all electronic components must be housed in water tight pressure housings (hereafter bottles). All of the

bottles used in the ingress vehicle are disposable so it was important to design them to minimize fabrication costs.

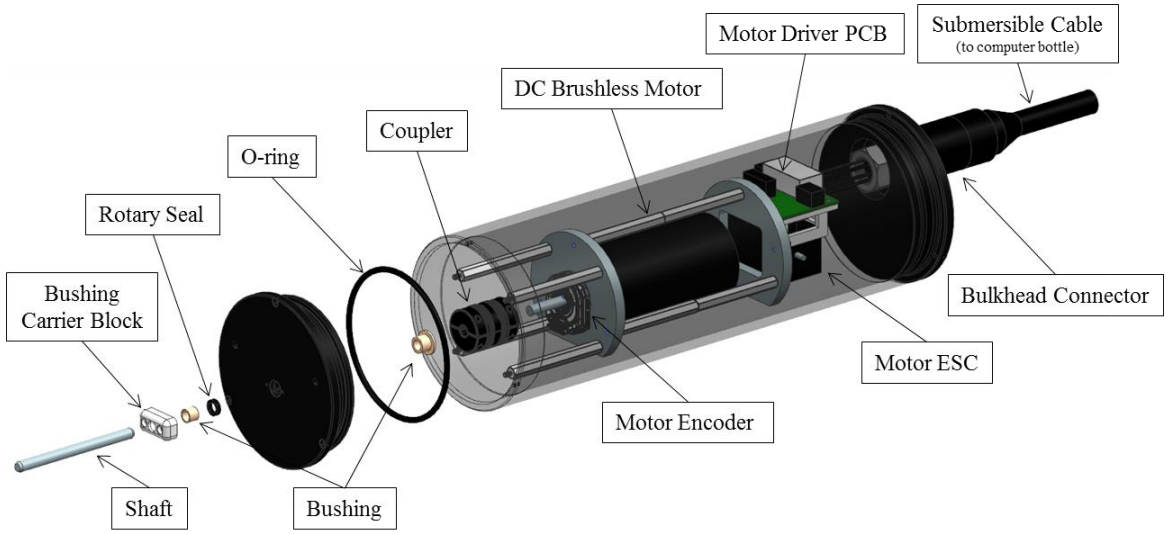

Figure 6.17 Partially exploded view of one of the motor bottles used in the TRSMAUV ingress vehicle.

Any generic bottle used in underwater applications generally consists of three components, which mate together to form the housing. The hull is a tube. This provides maximum strength against the large crush pressures experienced at depth. This tube section is sealed at both ends by bulkheads. There are two critical sealing surfaces in this bottle design. These are the two tube ends where they mate with the bulkheads. One or two piston o-rings are often used to seal the bottle. The merits of both one o-ring, and two o-ring configurations are discussed below (Section 6.6.2).

6.6.1 Tube Design

Weight is often a very critical design consideration when designing a tube section for use in an AUV. It is desirable to construct tube sections that have a minimum wall thickness for safe operation at the specified mission depth to minimize weight. Many tubes are designed with several internal ribs that are thicker than the overall wall thickness. The tube sections in the VT-SMAUV are designed this way. Although this is a proven method to reduce weight, it results in a very costly manufacturing process. The ingress vehicle, in contrast to the VT-SMAUV is a large scale disposable AUV. Thus, cheaper and heavier components are more desirable than lighter more expensive components.

The ingress vehicle tube sections were designed with minimum constant wall thickness. These tubes can be easily machined from stock tubing to reduce the overall cost. The tube sections

were designed with a large FoS so that machining tolerances could be enlarged for the inner and outer diameter to reduce cost. Small sections of the inside tube ends were designed with a very tight tolerance and specific surface finish to ensure a proper seal with the bulkheads [4].

Initial wall thicknesses of the motor bottle, actuator bottle and computer bottle were determined from simple FEA simulations performed on open ended tube sections. These results were then compared to results from calculations using the Von Mises yield equation [8]. Additionally each of these bottles was checked for elastic buckling. This calculation was performed by hand using equations relating the wall thickness, length, Young's modulus and the Poisson's ratio [8]. These three estimates provided enough information to select a safe wall thickness. For these designs a thickness was selected that would yield a desired FoS greater than two (Table 6.2).

Calculations using the Von Mises yield equation were performed using the same method described in the initial structural analysis of tube sections performed in [5]. This analysis determines a yield stress for crush failure based on the external pressure. The yield stress is calculated as the normal stress σ_T on the thin-wall tube. This normal stress is calculated from the three principal stresses on the tube (Fig. 6.18), using the Von Mises yield equation (6.4) [8]. These stresses (σ_1, σ_2, and σ_3 Fig 6.18) are found within the tube section as a result of the external pressure q of 750 psi [8]. The maximum stress σ_2 is determined at $r = r_{inner}$ and the maximum stress σ_3 is determined at $r = r_{outer}$, the total maximum stress location is unknown [8]. To account for this, the calculations were performed using ten different values of r, evenly spaced between r_{inner} and r_{outer}. The tensile yield stress σ_{yield} of aluminum 6061 was taken as 3.99×10^4 psi, and a FoS was determined for each bottle (Table 6.2). It is important to note that the crush FoS determined from these calculations assumes an infinite length tube. Therefore these FoS represent conservative estimates.

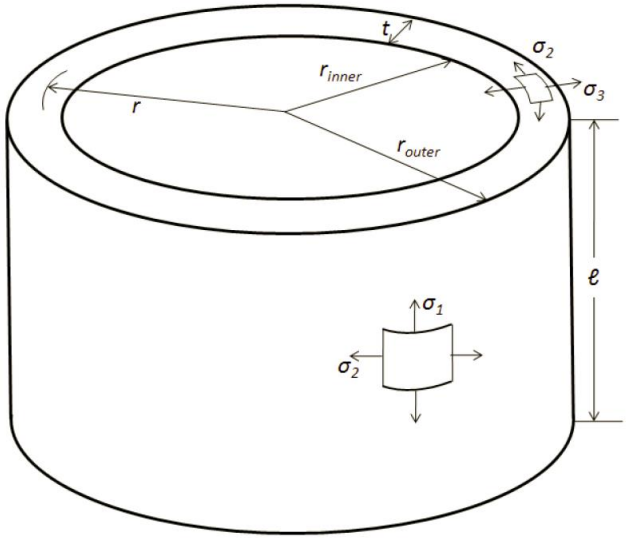

Figure 6.18 Dimensions and stress conventions of the tube stress analysis [8]

$$\sigma_1 = \frac{-qr_{outer}^2}{r_{outer}^2 - r_{inner}^2} \tag{6.1}$$

$$\sigma_2 = \frac{-qr_{outer}^2(r_{inner}^2 + r^2)}{r^2(r_{outer}^2 - r_{inner}^2)} \tag{6.2}$$

$$\sigma_3 = \frac{-qr_{outer}^2(r^2 - r_{inner}^2)}{r^2(r_{outer}^2 - r_{inner}^2)} \tag{6.3}$$

$$\sigma_T^2 = (\sigma_1^2 + \sigma_2^2 + \sigma_3^2) - \sigma_1\sigma_2 - \sigma_2\sigma_3 - \sigma_1\sigma_3 \tag{6.4}$$

$$FoS_{crush} = \frac{\sigma_{yield}}{\sigma_T} \tag{6.5}$$

To determine the FoS for elastic buckling, q' must first be calculated using Equation 6.6 [8]. In order to find q', the Young's modulus E and the Poisson's ratio v of the selected material are required (taken as 10.0×10^6 psi and 0.33 respectively for aluminum 6061). Additionally the wall thickness t and the length l of the tube must be selected. To use Equation 6.6 the number of lobes formed by the tube during buckling must be known. This is normally accounted for by solving for q' where $2 \leq n \leq 10$, and using the minimum value of q'. Based on experimental results, the recommended critical pressure P_{crit} occurs at 80 percent of the minimum value of q' [8]. The FoS for elastic buckling can then be found using P_{crit} and the expected external pressure q. From this calculation, it was clear that elastic buckling was not a concern for bottles of this size (Table 6.2).

$$q' = \frac{E\frac{t}{r_{outer}}}{1+\frac{1}{2}\left(\frac{\pi r_{outer}}{nl}\right)^2}\left[\frac{1}{n^2\left[1+\left(\frac{nl}{\pi r_{outer}}\right)^2\right]^2} + \frac{n^2t^2}{12r_{outer}^2(1-v^2)}\left[1+\left(\frac{\pi r_{outer}}{nl}\right)^2\right]^2\right] \tag{6.6}$$

$$P_{crit} = 0.80q' \tag{6.7}$$

$$FoS_{buckling} = \frac{P_{crit}}{q} \tag{6.8}$$

Table 6.2 Stress analysis results for bottle designs (FoS_{crush} based on infinite tube calculations and $FoS_{buckling}$ based on actual bottle lengths)

	Outer Diameter	**Length**	**Wall Thickness**	$\boldsymbol{FoS_{crush}}$	$\boldsymbol{FoS_{buckling}}$
Motor Bottle	4"	8.5"	0.2"	5.83	330
Computer Bottle	6"	14.5"	0.3"	2.59	335
Actuator Bottle	3.5"	8.5"	0.2"	8.92	414
Battery Bottle	6.9"	16.5"	0.25"	1.35	201

Both the motor bottle and the actuator bottle designs lead to very high factors of safety. It was not practical to have walls any thinner than 0.2". This is because threaded holes are placed at tube ends for bulkhead mounting. A stress analysis was not initially performed on the battery bottle. Instead, this bottle was designed with a wall thickness and diameter equal to the thickness of the original constant wall thickness tube sections from the VT-SMAUV [5]. A mistake was made during design and the battery bottle was fabricated with a wall thickness of 0.25" instead of the correct 0.4". Because of this error, the hand calculation strategy discussed above was used to determine the estimated FoS for both elastic buckling and crush. Initial calculations revealed that the battery bottle may not have the desired crush FoS (greater than 2) (Table 6.2). As stated earlier, the hand calculations generate a conservative estimate because they consider an infinite length tube. The two solid bulkheads at either end of the tube will significantly increase the strength of the tube section. A more in depth FEA simulation was performed with the bulkheads in place to determine a more accurate estimate for the crush FoS (Fig 6.19). For this simulation the tube and bulkheads were modeled as a single part. One end of the tube was constrained and an external pressure of 750 psi was applied to the bottle. Simulations were performed using several different mesh sizes until convergence was achieved. The final element size selected was 0.100" (Fig. 6.20).

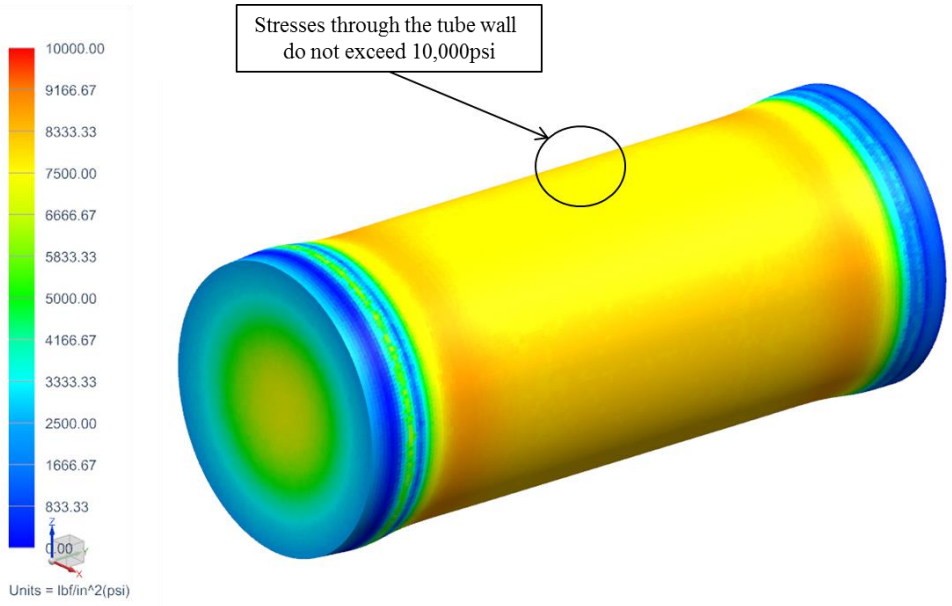

Figure 6.19 Battery bottle FEA simulation results

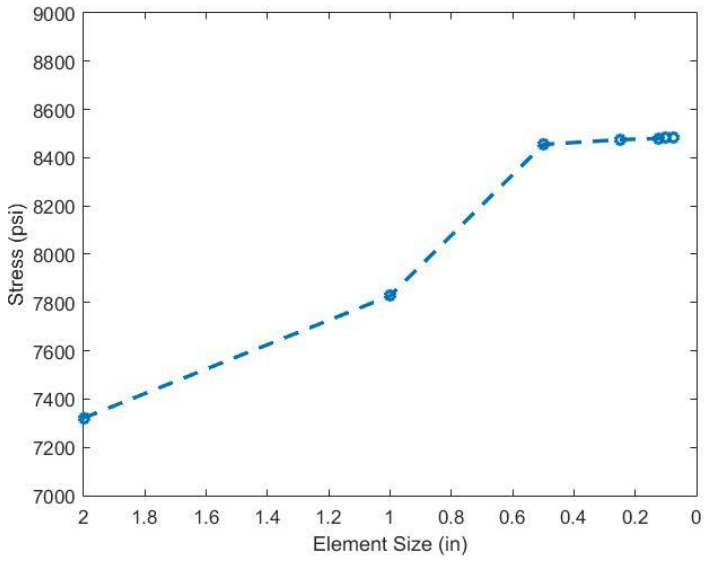

Figure 6.20 Mesh element size selection. The stress on the y-axis was averaged from several grid points selected at the tube center.

From this analysis it was observed that stresses through the wall in the tube section do not exceed 10000 psi. This simulation indicated that when assembled, the battery bottle will have a crush FoS = 4.2. For bottles of this size, the infinite tube analytical calculations produced very conservative estimates for crushing FoS.

6.6.2 Bulkhead Design

The bulkheads comprise the other components of the water tight hull. Often, a double o-ring seal is used in underwater mating application. This is beneficial when applied to mating surfaces that are frequently unsealed and resealed such as when access to a chamber is needed following each mission. A second o-ring adds extra security against wear on the o-rings. The o-ring groove that is machined into the mating surface of the bulkhead must be fabricated to an extremely tight tolerance and very fine surface finish [4]. It is important that the groove will not only complete the seal but will not damage the o-ring during installation. Many of the ingress vehicle bottles were designed with a single o-ring seal to minimize cost. The decrease in safety was acceptable because these bottles will not be subject to frequent opening and closing. A double o-ring seal was used in the battery bottle because the battery stack will be removed from the bottle for charging. This will lead to routine opening and closing of the battery bottle, and the second o-ring provides additionally security against leaks. A battery short could result in a serious explosion. A detailed structural analysis was not perfromed on the bulkheads. All of the bulkhead designs were closely based on previous designs in the VT-SMAUV and were thus assumed to have the required FoS.

6.6.3 Shaft and Seal Selection and Assembly

Bulkheads that have a shaft passing through them present another design difficulty. Constructing an effective seal around a rotating shaft is difficult and becomes increasingly difficult as hydrostatic pressure increases. A seal that is rated to great depth puts a large resistance on the shaft decreasing overall efficiency.

The majority of the ingress vehicle mission is completed at or near the surface (depth < 5 m). It is critical that the motors are operating at maximum efficiency during the ingress portion of the mission. The controlled portion of the ingress mission effectively ends at vehicle separation. For this reason, the seals that were initially selected are not rated to the mission depth of 500m. It was decided that minor flooding during the descent phase would be acceptable as long as motors and other components needed for control were not entirely flooded before separation occurs. The selection of these lower depth seals reduced the torque exerted on the shaft resulting in more efficient propulsion.

Careful consideration must be given to the shaft material and finish to maximize seal lifespan and efficiency. Increasing shaft hardness reduces friction and also reduces seal wear. This directly increases seal lifespan and propulsive efficiency. Applying a fine surface finish to the shaft is also important. Different finishes can increase or decrease the sealing ability of the rotary seal based on the fluid viscosity. Another important factor to consider is corrosion resistance of shaft material. Unfortunately, many of the most corrosion resistant materials are quite soft (e.g., 316 & 304 stainless steel (SS)). However, there are many surface coating options that increase hardness although these processes tend to be quite expensive. To keep cost at a minimum, 440c SS was selected for shafts that pass through seals. The 440c SS is much harder than other stainless steels but this comes with a reduced corrosion resistance. This reduction in corrosion resistance was not considered a problem because of the single mission requirement of the ingress vehicle. Shafts need not possess long endurance capabilities.

The design must provide adequate support for shafts passing through seals. Any misalignment or wobble in the shaft can lead to rapid seal wear and may prevent the seal from operating effectively to the rated pressure. For proper alignment and support, two bushings were positioned along the shaft, one on each side of the seal (Fig. 6.17). Plastic bushings were selected because they offered excellent wear resistance, minimal friction losses and had proved effective in previous vehicles. Another component often added to underwater vehicles is a shaft retainer (or thrust bearing). This is a component that absorbs the hydrostatic and thrust loading placed on the shaft so the load is not transmitted to the motor. This load can damage the motor or reduce efficiency, particularly at great depths. This component was left out of the initial design based again on the fact that the ingress vehicle is designed for single use and that the majority of operation occurs near the surface. However, sufficient space was left in the motor bottles to add a shaft retainer if it is found to be needed.

The shafts that pass through seals were designed to be just long enough to pass through the bulkhead. This design reduced the size of the precision shafts, reducing their cost. Each shaft is immediately coupled to an external shaft. Because these outer shafts do not pass through seals they were machined from 316 SS maximizing their corrosion resistance. During field trials, the 440c SS shafts and rotary seals may require routine replacement. With this design they can be easily replaced without having to disassemble the external linkage.

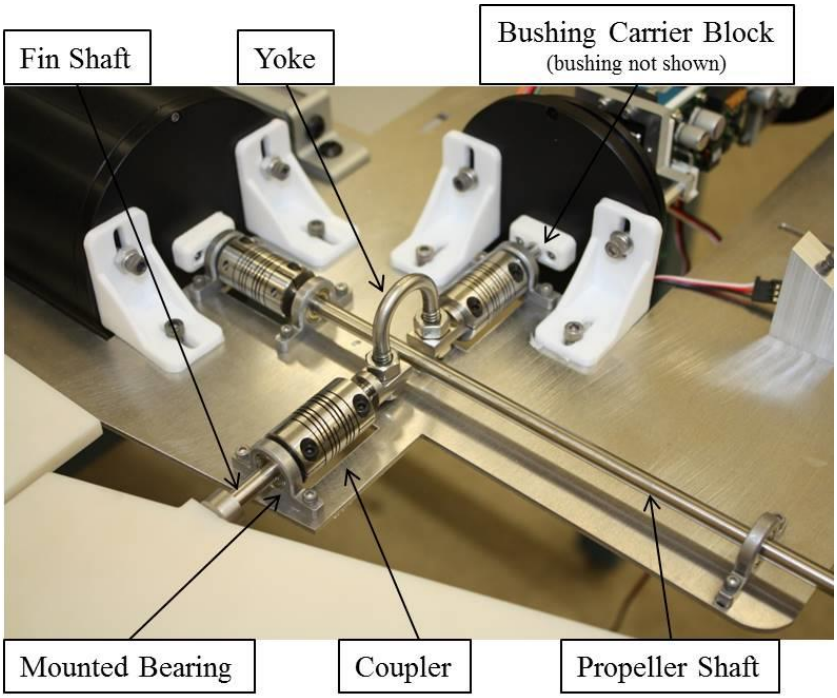

Figure 6.21 External linkage

It was beneficial to position the fin shafts and propeller shafts on the same plane. This required the addition of a shaft yoke where the shafts cross. A simple yoke assembly was constructed from a standard u-bolt fixed to flat ended shafts (Fig. 6.21). This assembly eliminated the need for expensive custom parts.

6.7 Shell

The shells used on the limited prototype were crude versions of the shells for the final vehicle. New shells were fabricated with more exact design specifications for the ingress vehicle prototype. These shells were designed to be used on the final vehicle as well as this prototype.

The overall shape of the shells remained the same but the internal composition was changed. The shell designed for the top half of the ingress vehicle was built to maximize buoyancy. This

reduced the amount of extra positive buoyancy that must be added to correctly balance the entire vehicle. This half is only required to be strong enough to maintain shape for consistent controlled flight. The bottom half shell is designed to maximize strength as it must deflect trawl cables and may be subject to impacts from other trawl equipment. Weight was not a concern for the bottom half because it must maintain a large bottom pressure while moored.

Both shells were made using a hybrid fiberglass and carbon fiber layup process. Layers of foam were sandwiched between the layers of fiberglass. This foam provides additional strength and buoyancy to the shell. Strips of carbon fiber were added to the shells along the edges and along the vertical spines to increase rigidity and strength. The composition of the shells along each edge is solid fiberglass and carbon fiber. This solid section of fiberglass and carbon fiber creates a seal around the internal foam, preventing it from absorbing water and adding weight.

The top half shell was partitioned into three pieces: A single forward portion (roughly ¾ the length of the vehicle), and an aft section split into starboard and port sections (Fig. 6.18). Clearance between the shell and internal components was only critical in the aft section of the vehicle. The forward section was designed to be thicker and more buoyant than the aft sections. Each of the aft sections was fabricated to be very thin in order to provide maximum space for the positioning of components inside this section of the vehicle. The bottom half shell was separated into two pieces: the removable top cap, and the fixed base (Fig. 6.22).

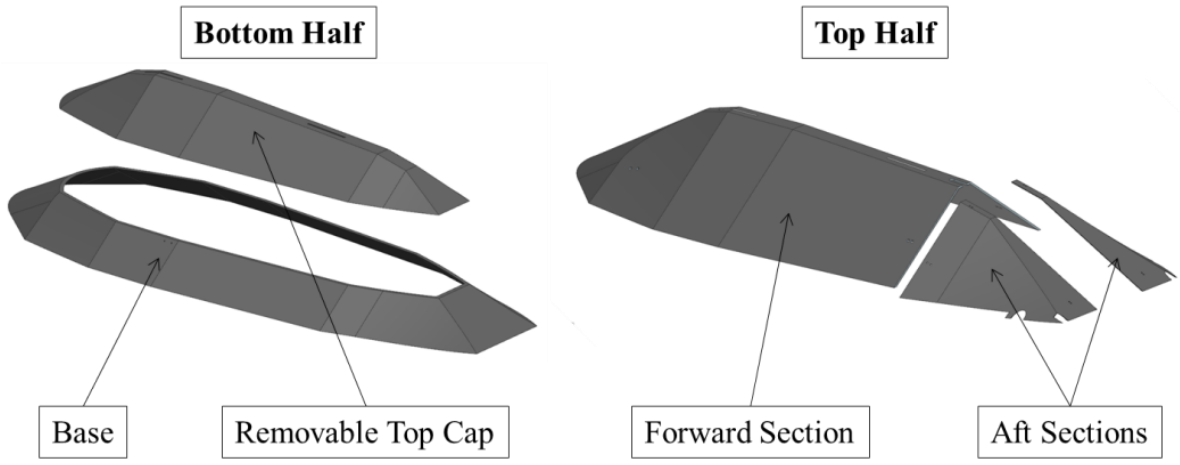

Figure 6.22 Ingress vehicle prototype shells

6.8 General Assembly

In a large vehicle like the ingress vehicle, consideration was given to the placement of every subsystem. Components were positioned so that many conditions could be met:

1. Correct weight and balance of vehicle
2. Ease of assembly
3. Easy accessibility to components that may require access in the field
4. Easy re-arming of buoyancy tubes and separation/attachment mechanism

The internal framing of this prototype was constructed from Aluminum T slotted extrusions. These frames were nearly identical to those used in the limited prototype (Section 4.4). The Aluminum T slotted framing allowed easy mounting of all subsystems and any additional weight or buoyancy required for vehicle ballasting.

All water tight bottles containing electronic components were positioned in close proximity and in the tail section of the vehicle. There are two identical motor bottles, a computer bottle and an actuator bottle. Each of these four bottles is mounted to a removable plate. All additional components of the propulsion and control surface systems are mounted to the plate as well (Fig. 6.23).

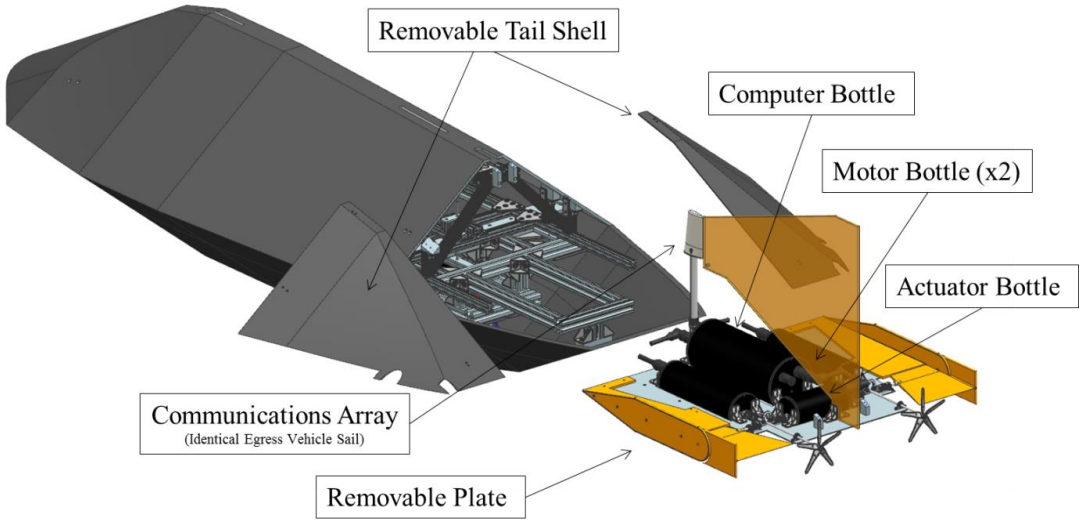

Figure 6.23 General layout for the ingress vehicle prototype

Overall assembly, bench testing and field repair were made more convenient with this mounting scheme. During benchtop testing, all systems that require extensive testing are mounted to the removable plate. This assembly is not as large and cumbersome as the full ingress vehicle. These components represent the most likely cause of failure in the field. They will be easily

accessible in the tail section of the ingress vehicle, and if necessary the entire plate can be removed from the vehicle to allow for comprehensive failure diagnosis and repair.

As noted in sections 6.1 and 6.3 both the skeg and the elevator assemblies may require size and shape modification to optimize performance. These components are mounted to the plate so that they are easily interchangeable with alternative designs. Additionally, for the ingress vehicle prototype the communication array is mounted directly in front of the skeg. With this mounting scheme a sail identical to that used on the egress vehicle could be used. This design reduced difficulty routing cables from antennas (in the communication array) to the modems (in the computer bottle).

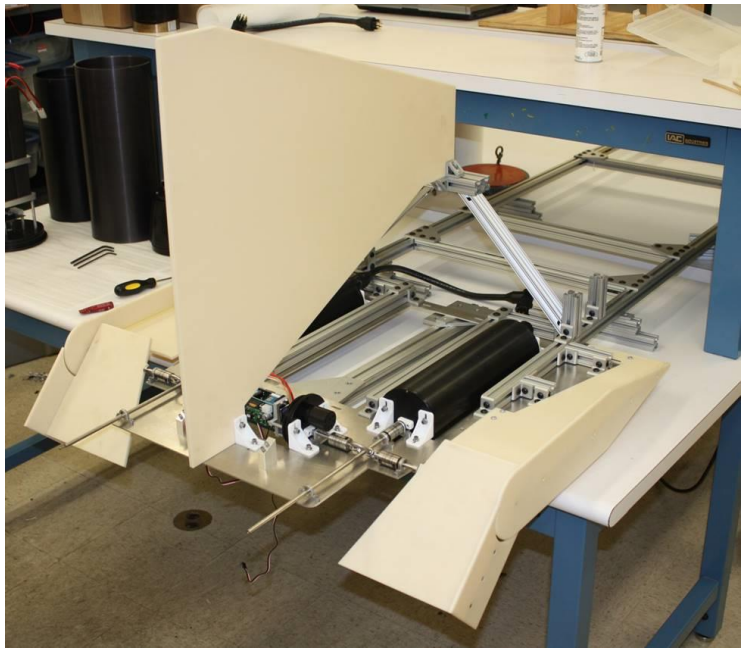

Figure 6.24 Ingress prototype

7 Next Phase

There is still a significant amount of work required to complete the TRSMAUV project. The ingress vehicle prototype is currently in the assembly phase. Upon full assembly of this prototype, the vehicle will undergo a rigorous field testing phase. Field testing will validate the flight ability of the ingress vehicle. Following confirmation that the ingress vehicle is capable of efficient controlled flight, detail design work will be completed for the top-cap release of the bottom half mooring mount. Additionally, detail design will be completed for mounting the egress vehicle inside the ingress vehicle. This system will be fabricated and installed into the ingress vehicle prototype. The final stage of the TRSMAUV design process will be full scale mission testing that will include all stages of the mission profile.

8 References

[1] JG Dessureault, DJ Belliveau, SW Young, "Design and Tests of a Trawl-Resistant Package for an Acoustic Doppler Current Profiler", IEEE Journal of Oceanic Engineering, **16**(4):397-401, 1991.

[2] SC Cumbee, "A New Trawl-Resistant Bottom Mount to Support Hydrographic Current Measurement Requirements", OCEANS 2001, Honolulu, HI, 2001

[3] H Perkins, F de Strobel, and L Gualdesi, "The Barny Sentinel Trawl-Resistant ADCP Bottom Mount: Design, Testing, and Application", IEEE Journal of Oceanic Engineering, **25**(4):430-436, 2000.

[4] "Parker O-Ring Handbook", Parker Hannifin Corporation, Cleveland, OH, 2007.

[5] Briggs, Robert C. *Mechanical Design of a Self-Mooring Autonomous Underwater Vehicle.* Thesis. Virginia Polytechnic and State University, 2010

[6] Ball, Eddie, personal communication, November 17, 2015

[7] Portner, Stephen, personal communication, May 12, 2015

[8] Young, W.C., *Roark's Formulas for Stress & Strain*, McGraw-Hill, Inc., New York, NY 1989.

[9] Mooring Systems, Inc, "Bottom Mount Systems for ADCPS", August 2015. Online. [Available] http://www.mooringsystems.com/mounts.htm